Lewis Research
IN-72-CR
191955
58 p.

NASA CR - 182238

NASA

THE DIVERGENCE CHARACTERISTICS OF CONSTRAINED-SHEATH OPTICS SYSTEMS FOR USE WITH 5-eV ATOMIC OXYGEN SOURCES

Prepared for

LEWIS RESEARCH CENTER

NATIONAL AERONAUTICS AND SPACE ADMINISTRATION

Grant NAG 3-791

Final Report

by

John R. Anderson

January 1989

Approved by

Paul J. Wilbur
Department of Mechanical Engineering
Colorado State University
Fort Collins, Colorado 80523

(NASA-CR-182238) THE DIVERGENCE CHARACTERISTICS OF CONSTRAINED-SHEATH OPTICS SYSTEMS FOR USE WITH 5-eV ATOMIC OXYGEN SOURCES Final Report, Apr. 1987 - Sep. 1988 (Colorado State Univ.) 58 p CSCL 20H G3/72

N89-19973

Unclas
0191955

NASA
National Aeronautics and Space Administration

Report Documentation Page

1. Report No.	2. Government Accession No.	3. Recipient's Catalog No.
NASA CR-182238		

4. Title and Subtitle
THE DIVERGENCE CHARACTERISTICS OF CONSTRAINED-SHEATH OPTICS SYSTEMS FOR USE WITH 5-eV ATOMIC OXYGEN SOURCES

5. Report Date
Jan. 1989

6. Performing Organization Code

7. Author(s)
John R. Anderson and Paul J. Wilbur

8. Performing Organization Report No.

10. Work Unit No.

9. Performing Organization Name and Address
Department of Mechanical Engineering
Colorado State University
Fort Collins, CO 80523

11. Contract or Grant No.
NAG 3-791

13. Type of Report and Period Covered
Final
April 87 - Sept. 88

12. Sponsoring Agency Name and Address
National Aeronautics and Space Administration
Washington, D.C. 20546

14. Sponsoring Agency Code

15. Supplementary Notes
Grant Monitor - Sharon Rutledge
NASA Lewis Research Center
Cleveland, OH 44135

16. Abstract

The potential usefulness of the constrained-sheath optics concept as a means of controlling the divergence of low energy, high current density ion beams is examined numerically and experimentally. Numerical results demonstrate that some control of the divergence of typical ion beamlets can be achieved at perveance levels of interest by contouring the surface of the constrained-sheath properly. Experimental results demonstrate that a sheath can be constrained by a wire mesh attached to the screen plate of the ion optics systems. The numerically predicted beamlet divergence characteristics are shown to depart from those measured experimentally, and additional numerical analysis is used to demonstrate that this departure is probably due to distortions of the sheath caused by the fact that it attempts to conform to the individual wires that makes up the sheath constraining mesh. The concept is considered potentially useful in controlling the divergence of ion beamlets in applications where low divergence, low energy, high current density beamlets are being sought, but more work is required to demonstrate this for net beam ion energies as low as 5 eV.

17. Key Words (Suggested by Author(s))	18. Distribution Statement
Ion Beam Focusing Atomic Oxygen Test Facility	Unclassified - Unlimited

19. Security Classif. (of this report)	20. Security Classif. (of this page)	21. No of pages	22. Price*
Unclassified	Unclassified	58	

NASA FORM 1626 OCT 86

*For sale by the National Technical Information Service, Springfield, Virginia 22161

TABLE OF CONTENTS

Section	Page
INTRODUCTION	1
BACKGROUND	3
COMPUTER PROGRAM	13
COMPUTER MODELING RESULTS	16
OPTICS SYSTEM SCALING EXAMPLE	38
COMPARATIVE EXPERIMENTAL STUDY	40
Experimental Apparatus	40
Preliminary Experimental Results	44
CONCLUSIONS	51
REFERENCES	53
DISTRIBUTION LIST	54

LIST OF FIGURES

Figure		Page
1	Discharge Chamber and Typical Ion Optics System.....	4
2	Constrained-Sheath Optics System and Beamlet Divergence Angle.....	7
3	Standard Grid Geometry Showing Radii of Curvature of Sheath-Constraining Mesh Geometries Studied.....	17
4	Beamlet Trajectories through a Single Aperture Constrained-Sheath Optics System Operating at Three Different Perveance Values.....	18
5	Computer Generated Divergence Angle Data for r_c/d_s = 0.575 and ℓ_g/d_s = 0.5 Constrained-Sheath Optics System.....	23
6	Computer Generated Divergence Angle Data for r_c/d_s = 0.665 and ℓ_g/d_s = 0.5 Constrained-Sheath Optics System.....	24
7	Computer Generated Divergence Angle Data for r_c/d_s = 0.75 and ℓ_g/d_s = 0.5 Constrained-Sheath Optics System.....	25
8	Computer Generated Divergence Angle Data for r_c/d_s =1.25 and ℓ_g/d_s = 0.5 Constrained-Sheath Optics System.....	26
9	Computer Generated Divergence Angle Data for r_c/d_s = 25 and ℓ_g/d_s = 0.5 Constrained-Sheath Optics System.....	27
10	Computer Generated Divergence Angle Data for r_c/d_s = 0.5125 and ℓ_g/d_s = 0.25 Constrained-Sheath Optics System.....	31
11	Computer Generated Divergence Angle Data for r_c/d_s = 0.575 and ℓ_g/d_s = 0.25 Constrained-Sheath Optics System.....	32
12	Computer Generated Divergence Angle Data for r_c/d_s = 0.75 and ℓ_g/d_s = 0.25 Constrained-Sheath Optics System.....	33
13	Computer Generated Divergence Angle Data for r_c/d_s = 1.25 and ℓ_g/d_s = 0.25 Constrained-Sheath Optics System.....	34
14	Computer Generated Divergence Angle Data for r_c/d_s = 0.575 and ℓ_g/d_s = 1 Constrained-Sheath Optics System.....	35

Figure		Page
15	Computer Generated Divergence Angle Data for r_c/d_s = 0.75 and ℓ_g/d_s = 1 Constrained-Sheath Optics System	36
16	Computer Generated Divergence Angle Data for r_c/d_s = 1.25 and ℓ_g/d_s = 1 Constrained-Sheath Optics System	37
17	Discharge Chamber and Optics System	41
18	Faraday Probe	43
19	Comparison of Experimental and Computer Generated Divergence Angle Data for Constrained-Sheath Optics System	46
20	Variation in Initial Ion Velocity and Sheath Boundary Geometry at High and Low Plasma Densities	48
21	Beamlet Trajectories with Initial Velocity Distribution through a Constrained-Sheath Optics System Operating at 0.23 Normalized Perveance Per Hole	50

INTRODUCTION

Space tests have demonstrated that oxygen atoms strike the surfaces of spacecraft in low earth orbit at a sufficiently high rate to cause some spacecraft materials to erode rapidly.[1,2] The speed of these atoms relative to the spacecraft, which is determined by the spacecraft orbital speed, corresponds to an oxygen atom kinetic energy of about 5 eV. In order to evaluate the suitability of various spacecraft materials that might be exposed to this oxygen flux, it is desirable to make an earth-based test facility that can produce a broad beam of 5 eV oxygen atoms at fluxes corresponding to those found in space so they can be directed onto samples of various materials. A system capable of doing this might include 1) a discharge chamber in which atomic and molecular oxygen ions are produced, 2) an ion extraction system that draws a beam of these ions from the chamber at the desired energy and current density, 3) a mass discrimination system that removes the unwanted molecular oxygen component from the beam, and 4) a charge exchange cell where the atomic oxygen ion beam exiting the mass discriminator is converted into a neutral atomic oxygen beam.

Although all four subsystems listed above are important components of an effective 5 eV atomic oxygen test facility, this report will focus on one of them--the ion extraction or ion optics subsystem. This subsystem is being addressed first because the extraction of a high current density, broad, low energy, low divergence ion beam is considered to require a substantial extension of ion optics technology and as a result it has been identified as limiting. It is noted in partial support of this order of priorities that an experiment

conducted during the grant period demonstrated that a discharge chamber can be operated using oxygen as a source gas. Since oxygen ions can be produced and provided to the optics subsystem, it is also considered logical to study the subsystem that forms the beam as the next element in the system sequence. If the desired beam can be produced, work to optimize the mass discrimination subsystem and to determine acceptable charge exchange cell operating conditions can proceed.

A beam of low energy ions is needed in this application to simulate, as closely as possible, the environment found in space. Also, at the target, the atomic oxygen current density produced by the overall system should be sufficiently high so that it approaches the conditions observed in space (on the order of 0.1 mA eq/cm^2). In order to overcome losses that will occur in the mass discrimination and charge exchange subsystems and still satisfy this final current density condition, the actual density extracted from the optics system must be considerably greater than this value. How much greater is determined in part by the extent to which a low divergence beam (i.e. one that will contain a minimum number of ions that will be lost on errant trajectories) can be produced. In this regard, it is noted that an ideal ion beam would be one in which all extracted ions would travel on parallel trajectories after passing through the optics subsystem.

Although there are many ion optics concepts, the constrained-sheath concept, described in Ref. 3, was identified as a promising one for producing the required low energy, low divergence, high current density ion beam. A computer program was developed to aid in evaluation of various constrained-sheath optics system geometries and

operating conditions. The most promising cases could then be selected for eventual experimental evaluation. Numerically generated optics performance predictions obtained using this computer program together with preliminary experimental results will be presented in this report.

BACKGROUND

A typical ion optics subsystem of the type studied in this report consists of two parallel plates each of which contains a hole through which the ion beam is extracted in the manner suggested in Fig. 1. A single pair of aligned holes has been used in this study for both the numerical and experimental studies although many pairs of holes would probably be used in an actual atomic oxygen simulation system. One of the plates (the screen plate in Fig. 1) is attached directly to one end of the discharge chamber. The other plate (the accel plate) is held a prescribed distance away from the screen plate on insulating supports. Insulating supports serve to isolate the screen and accel plates electrically, both from each other and from ground, so the accel and screen plates can be biased negative and positive, respectively, relative to ground potential. The electric field set up between these biased plates causes ions to be drawn out of the discharge chamber, while electrons attempting to leave are reflected back into the discharge chamber plasma. The zone in which this reflection occurs is called the sheath, and it is frequently assumed that the sheath separates a region where the ions and electrons do not feel large electric field forces (the discharge plasma region) from

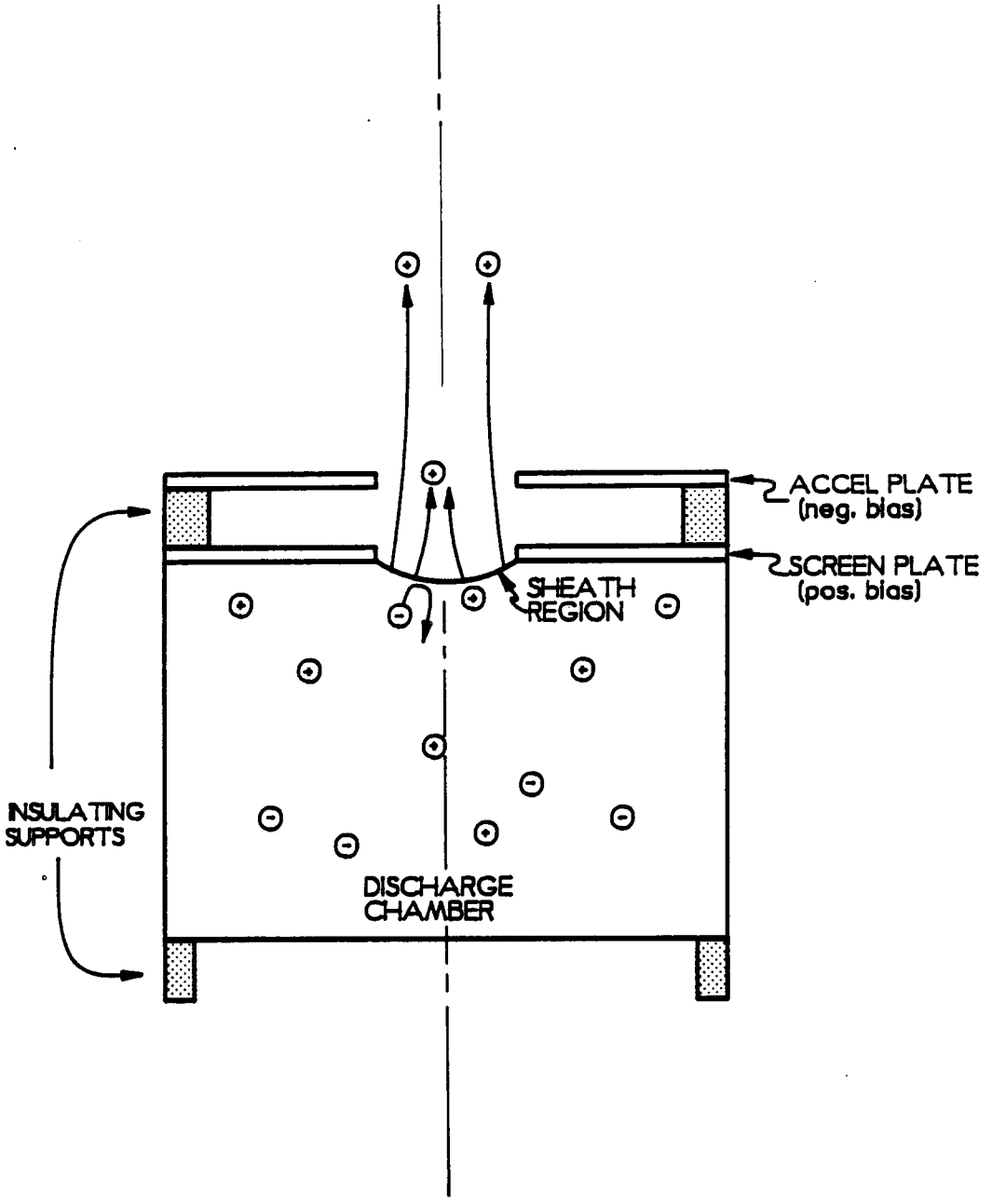


Fig. 1. Discharge Chamber and Typical Ion Optics System

one where the ions feel the full acceleration force induced by the electric field applied between the plates (the intraplate region).

The divergence behavior of an ion beam is determined by the trajectories of the individual ions within the beam and these trajectories are determined, in turn, by the electric field forces that act on the ions as they pass from the sheath through the accel plate. The contour of the sheath has a particularly strong influence on these trajectories because it determines the direction of these forces during the early phase of the acceleration process when ion velocities are low. In traditional (free-sheath) ion optics systems, the sheath takes on the shape dictated by the natural requirement that the rate at which ions are supplied to the sheath from the discharge plasma be equal to the rate at which they can be accelerated and extracted through the optics system. This requirement must be met at all operating conditions, and as a consequence changes in such conditions as the intraplate electric field or the discharge chamber plasma density cause the sheath to change its shape. As a result the sheath shape cannot be controlled independent of ion energy and current density conditions in a free-sheath optics system.

Constrained-sheath optics systems have been suggested[3] as an alternative to free-sheath optics that would help control the sheath shape independent of operating conditions and thereby facilitate ion beam divergence control. The idea behind the constrained-sheath concept is to place a constant potential physical boundary between the plasma in the discharge chamber and the intraplate region in the form of a wire mesh covering the screen plate aperture. Such a wire mesh does indeed provide some divergence control; however, as will be discussed, space-charge effects, which arise because particles with

like charge repel each other, limit divergence control at high beam current densities. Also, the spacing between the wires in such a mesh and their diameter appear to affect beam divergence.

In order to produce the broad beam of 5 eV oxygen atoms to bombard large targets, a multiple-aperture optics system will be needed. The divergence characteristics of such beams will not be studied here because it is recognized that the divergence behavior of multiple aperture systems can be determined by summing techniques, if the divergence behavior of a single beamlet extracted through a screen/accel plate hole pair is known. Therefore, divergence characteristics will be determined using the simpler single aperture pair system.

Figure 2 shows the basic geometry of a two-plate, constrained-sheath optics system. The screen and accel plates are shown with coaxial circular holes and a sheath constraining mesh is shown attached to the screen plate. The most divergent of the ions being extracted define an envelope of the beamlet that looks something like the one shown in Fig. 2. As this envelope suggests, the ions generally begin their trajectories at the constrained sheath with a radially inward-directed velocity component but the forces acting on them as they travel through the optics system tend to cause them to diverge (i.e. travel on radially outward-directed trajectories). Neutralizing electrons are injected into the beamlet downstream of the accel plate and because of this a neutralization surface like the one shown in Fig. 2 develops. Downstream of this surface a uniform potential plasma exists, the electric field forces on the ions drop to zero and the ions travel on linear trajectories. If electrons were not injected to neutralize the beam, the mutual repulsion between the

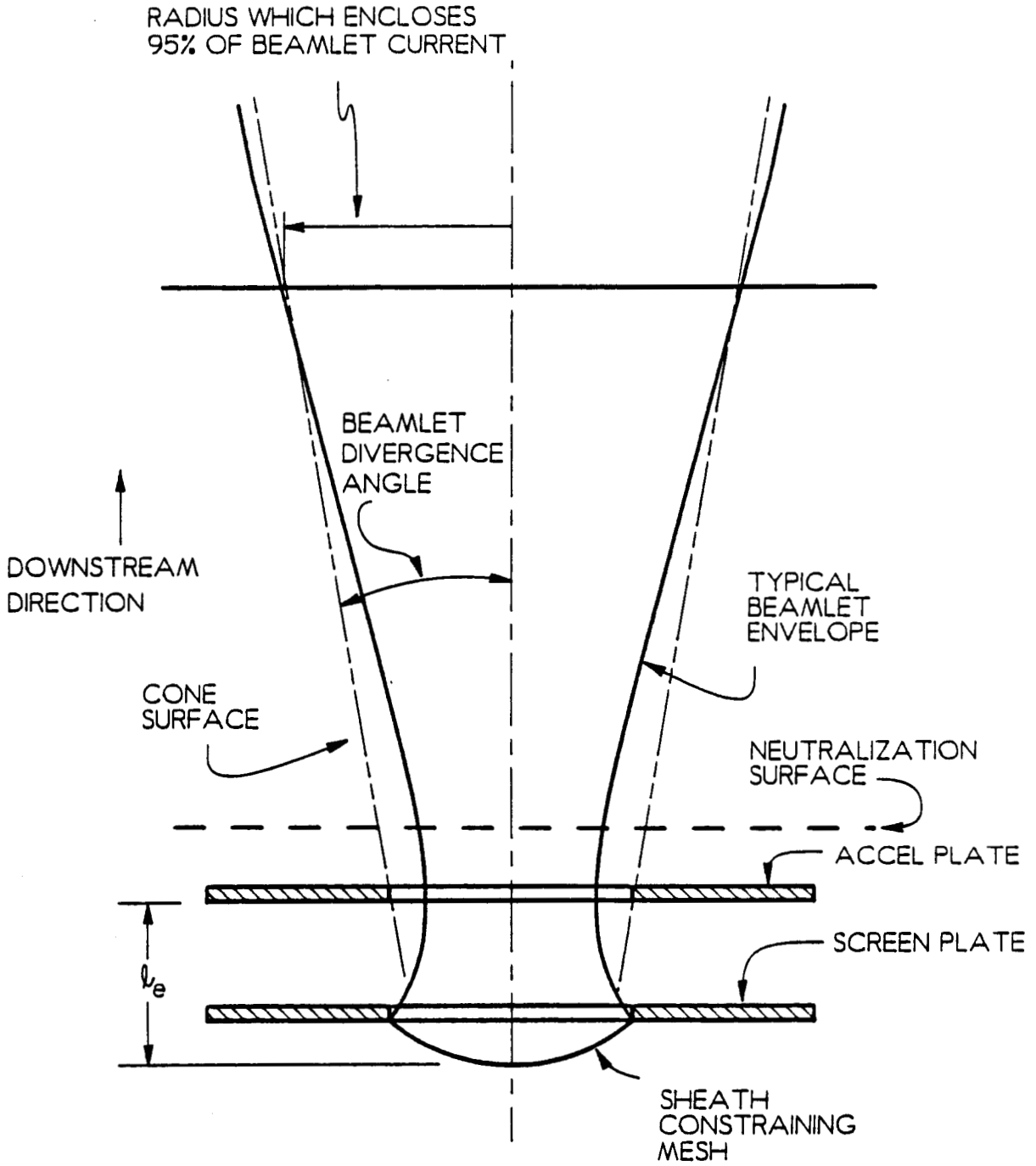


Fig. 2. Constrained-Sheath Optics System and Beamlet Divergence Angle

positively charged ions would cause continued beamlet divergence at all locations downstream of the accel plate. To keep the beamlet neutralizing electrons from traveling upstream into the discharge chamber--a condition which would waste power and might cause the discharge chamber to overheat--the accel plate potential is maintained below the potential of the neutralized beamlet. It is at the points where electrons feel the effect of the potential on the accel plate and are repelled that the boundary separating the neutralized and unneutralized portions of the ion beamlet (the neutralization surface) develops.

The beamlet divergence angle is also defined in Fig. 2 as the half angle of the right circular cone arranged so its surface intersects both the circle enclosing 95% of the beamlet current in a plane located downstream of the neutralization surface and the downstream circumference of the accel plate hole. This definition arises from practical considerations in experimental work which necessitate the measurement of ion beamlet current density profiles at some finite distance downstream of the plates and from the fact that the accel hole represents to first order the beamlet source. In practice the cone shown in Fig. 2 is defined by the accel plate hole and a circle in the plane where the current density is measured. This circle is found by measuring the beamlet current density profile at a plane of interest, integrating this profile and then determining the radius of the circle, coaxial with the beamlet centerline in this plane, that encloses 95% of the beamlet current. From Fig. 2, it is evident that the beamlet is more divergent than the angle computed from the definition; however, the discrepancy becomes smaller as the distance

between the accel plate and the axial location where the beamlet current density profile is measured increases.

Although it is evident from Fig. 2 that at least two dimensions (namely, the radial and axial ones) are needed to model an optics system accurately, a parameter which proves useful for describing ion beamlets can be obtained from a simple, one-dimensional model. This model describes the current of particles with like charge flowing between two parallel conducting plates at different potentials. These plates represent the screen plate as a source of zero velocity particles and an accel plate that collects them. Although the model is valid for either positive or negative particles, for this discussion it will be assumed that they are positive ions. The maximum current of ions (J_M) that can flow in this situation is limited to a value determined by the area of the plates (A), the charge-to-mass ratio of the ions (q/m_i), the separation distance between the plates (ℓ_e) and the potential difference applied between them (V_T) through the Child-Langmuir law.[4]

$$J_M = \frac{4}{9} \epsilon_0 \sqrt{\frac{2q}{m_i}} V_T^{3/2} \frac{A}{\ell_e^2} \tag{1}$$

Here ϵ_0 is the permittivity of free space and q is the particle charge which will be assumed equal to one electronic charge. If the beamlet cross-sectional area is circular (as is the case with the optics systems studied in this report) with diameter d_s, Eq. 1 can be rewritten as

$$\frac{J_M}{V_T^{3/2}} = \frac{\pi}{9} \epsilon_0 \sqrt{\frac{2q}{m_i}} \left[\frac{d_s}{\ell_e}\right]^2 . \qquad (2)$$

The term on the right-hand side of Eq. 2 is dependent only on geometry and the charge-to-mass ratio of the ions and for a given optics system operating on a given gas these quantities do not change. Under these conditions the right-hand side of Eq. 2 is constant and a useful parameter, called normalized perveance per hole, can be obtained by dividing the left-hand side of Eq. 2 by the right-hand side to obtain

$$P = \frac{J_B}{V_T^{3/2}} \left[\frac{\ell_e}{d_s}\right]^2 \left[\frac{\pi}{9} \epsilon_0 \sqrt{\frac{2q}{m_i}}\right]^{-1} . \qquad (3)$$

Here J_B, the actual current flowing between the plates, can range from zero (for which $P = 0$) to the space-charge limited current J_M (for which $P = 1$).

In order to extract ions through a real optics system, both the screen and accel plates must have holes in them and a one-dimensional model of the acceleration process cannot provide accurate beamlet divergence information. The above definition of normalized perveance per hole can still be used, however, if some of the terms that appear in it are appropriately redefined. Specifically, the total accelerating voltage is redefined as the difference between the discharge chamber plasma and accel plate potentials. This potential difference is used because ions entering a constrained-sheath optics system accelerate from the constraining sheath until they reach the

accel plate hole. It is noted in support of this definition that ions decelerate after they pass through the accel plate because the potential of the neutralization surface is above that of the accel plate and the Child-Langmuir limit is applied only through the region of acceleration. The effective acceleration distance (ℓ_e), sought for Eq. 3, is the mean distance through which ions are accelerated between the constrained sheath and the minimum potential points on their trajectories. A reasonable estimate of this distance is considered to be the axial distance between the furthest upstream point on the constraining sheath and the upstream plane of the accel plate as shown in Fig. 2. The quantity d_s is the screen hole diameter and the rest of the terms used in Eq. 3 are the same as those for the one-dimensional model.

Before commenting on the usefulness of normalized perveance per hole, hereafter referred to as perveance, two more important parameters--net ion energy (V_N) and net-to-total accelerating voltage ratio (R)--must be defined. Net ion energy is the kinetic energy that an ion acquires in passing through the optics system (i.e. passing from the discharge plasma to the neutralization surface). It is computed as the product of the ion charge and the difference between the discharge plasma potential and the potential of the plasma downstream of the neutralization surface. When expressed in eV the net energy of a singly charged ion is numerically equal to the net accelerating voltage. The net-to-total accelerating voltage ratio is defined by

$$R = \frac{V_N}{V_T} \quad . \tag{4}$$

Perveance and net-to-total accelerating voltage ratio are particularly important parameters because holding them constant enables one to scale an optics system with fixed geometrical ratios and the associated beamlet divergence angle will remain unchanged. Because of this, beamlet divergence experiments can be conducted using optics systems that are convenient to both construct and instrument for beamlet divergence measurements and the results obtained can be used to predict the performance of geometrically similar grids under different operating conditions. In order to facilitate such optics system geometrical scaling, optics system dimensions will be non-dimensionalized using the screen plate hole diameter and beamlet divergence data will be plotted as functions of perveance and net-to-total accelerating voltage ratio.

Another useful consequence of perveance scaling is that preliminary experiments can be conducted using an inert gas, such as argon, instead of oxygen which is reactive and therefore less convenient to use, and the results can be used to predict oxygen beamlet divergence behavior. Once the optics system geometry that gives the desired beamlet divergence characteristics has been found, the desired beamlet current density can be obtained by manufacturing plates that reflect the scaling law inherent in Eq. 3 (i.e. the one having an effective acceleration length ℓ_e that will yield this current density at the design net accelerating voltage V_N and the charge-to-mass ratio q/m_i of the design source gas). Of course, final experiments should be conducted using oxygen and the plates designed to produce the desired current densities so second-order effects neglected in the scaling process can be reflected in the final design.

COMPUTER PROGRAM

A computer program was developed to model the phenomena occurring in single aperture pair, constrained-sheath optics systems. The computer program uses a physical model similar to the one described in Refs. 5 and 6. Although the equations used in the model are described in detail in Refs. 5 and 6, a brief description of the physics used in the computer model is given here. The model uses the Lorentz force law

$$\mathbf{F} = q\,[\,\mathbf{E} + \mathbf{v} \times \mathbf{B}\,] \tag{5}$$

to compute ion trajectories. Here $\mathbf{F}$ is the vector force acting on the charged particle, q is the particle charge, $\mathbf{E}$ is the vector electric field strength, $\mathbf{v}$ is the vector particle velocity and $\mathbf{B}$ is the vector magnetic flux density. In the optics systems being studied, the forces due to magnetic fields are several orders of magnitude smaller than forces due to electric fields and they are therefore ignored. Thus, the Lorentz force law, as used in the model, reduces to

$$\mathbf{F} = q\,\mathbf{E} \quad . \tag{6}$$

Other assumptions included in the model are that no particle collisions occur while the ions are passing through the optics system, the current density is uniform over the surface of the constraining sheath, and the neutralization surface is planar. Another assumption, which will be expanded upon later, is that ions leave the surface of the constraining sheath and enter the intraplate region traveling

perpendicular to this surface. The program assumes axial symmetry and the analysis is executed using a planar grid that has been overlaid on an axial cross section through the center of a constrained-sheath optics set of interest.

The potential at each grid point can be computed using Poisson's equation for electrical potential fields

$$\nabla^2\varphi = \rho/\epsilon_0 \tag{7}$$

where φ is electrical potential, ρ is electrical charge density and ϵ_0 is the permittivity of free space. This equation is actually applied in the computer model in axisymmetric, cylindrical coordinate, finite difference form. It is first used to compute potentials at each grid point using a relaxation technique for the case where zero electrical charge density exists at each mesh point and the plates and sheath constraining surface have the prescribed boundary values of interest (i.e. the Laplace equation solution to the problem is obtained). Once a potential field has been determined, the trajectory of an ion coming from a prescribed position on the sheath, having an initial velocity normal to the constrained-sheath surface which is determined by the discharge plasma/screen plate potential difference, is computed. This is accomplished by determining electric field vectors (values of the gradient of the potential field) at the location of the ion and then applying Newton's 2nd Law and a conservation of particle energy expression to determine, sequentially and repetitively, the particle acceleration, velocity and position relative to the radial and axial grid points. Because particle trajectories generally do not pass precisely over mesh points this procedure is applied using an

interpolating routine to determine forces at points located between grid points. The trajectory computation procedure is repeated several times to determine trajectories for ions drawn from various points on the constrained-sheath surface.

Adjacent trajectories define the boundaries of current-carrying stream tubes and a charge density determined by the current density being supplied at the constrained sheath is assigned to each mesh point that falls inside these stream tubes. Once this space-charge distribution has been determined, the finite difference form of Eq. 7 is reapplied considering the charge density assigned to each mesh point (i.e. Poisson's equation is applied) and a new electric potential distribution is computed. Since this will result in a different potential field than the initial one, ion trajectories will be different than they were for the initial computation and they must be recomputed. The process of recomputing trajectories, reassigning charge density to mesh points falling inside associated stream tubes and then recomputing electrical potentials and ion trajectories is repeated until convergence is realized (i.e. until the potential field distribution no longer changes significantly when trajectories are recomputed).

After convergence has been achieved, the beamlet current density can be computed at locations downstream of the neutralization surface. This is done by following straight line ion trajectories from the neutralization surface to the location where the beamlet current density is to be determined. The current density is determined by the current flowing between adjacent trajectories and the cross-sectional area through which it is flowing. Once the beamlet current density profile has been computed, it can be integrated, the circle enclosing

95% of the beam current can be found and the beamlet divergence angle can be computed in accordance with the definition given previously.

COMPUTER MODELING RESULTS

The computer program was used to map out the divergence characteristics of ion beamlets, as a function of perveance, for various net-to-total accelerating voltage ratios and various constrained-sheath optics system geometries. In order to do this in a systematic way that would be amenable to logical data presentation, a plate system geometry, accel plate potential and discharge plasma potential were defined as typical or standard and the effects introduced by changing beam current, constrained-sheath radius of curvature and screen plate potential for this standard case were investigated. Figure 3 shows the standard geometry involved a screen aperture diameter d_s of 2 cm and $\ell_g/d_s = \ell_n/d_s = 0.5$, $d_a/d_s = 1$ and $t_s/d_s = t_a/d_s = 0.05$. Here ℓ_g is the separation distance between the screen and accel plates, ℓ_n is the distance between the accel plate downstream surface and the neutralization surface, d_a is the accel plate aperture diameter, t_s is the screen plate thickness and t_a is the thickness of the accel plate. As Fig. 3 suggests, the radius of curvature was varied from the value for a full hemisphere ($r_c/d_s = 0.5$) to that for an almost flat ($r_c/d_s = 25$) constrained sheath.

To gain some insight into the phenomena occurring in a constrained-sheath optics system, it is useful to examine Fig. 4. This figure shows ion beamlets being extracted through an optics system at three different perveance levels ($P = 0.002$, $P = 0.2$ and $P = 0.45$). Shown are the screen and accel plates, the neutralization

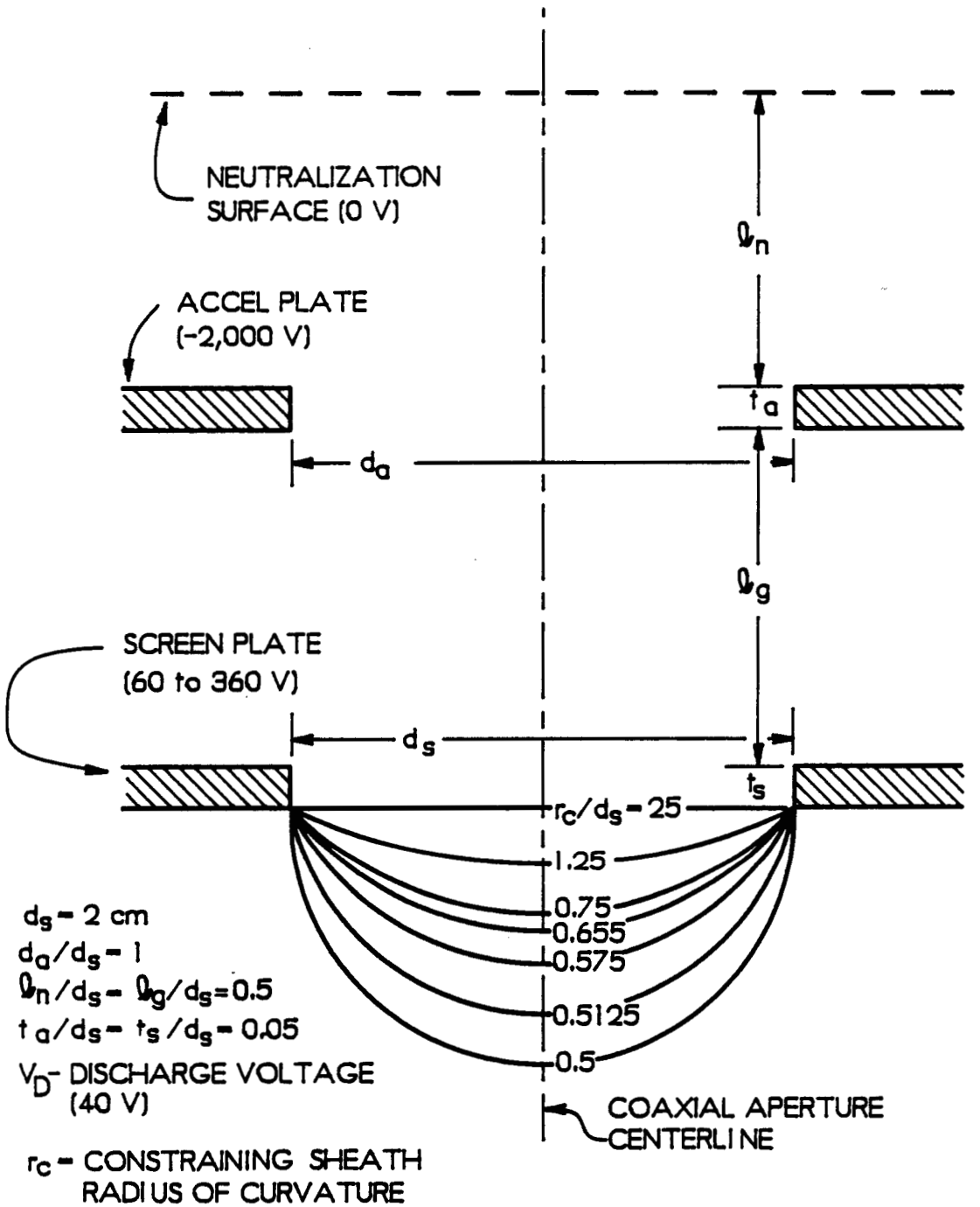


Fig. 3. Standard Grid Geometry Showing Radii of Curvature of Sheath-Constraining Mesh Geometries Studied

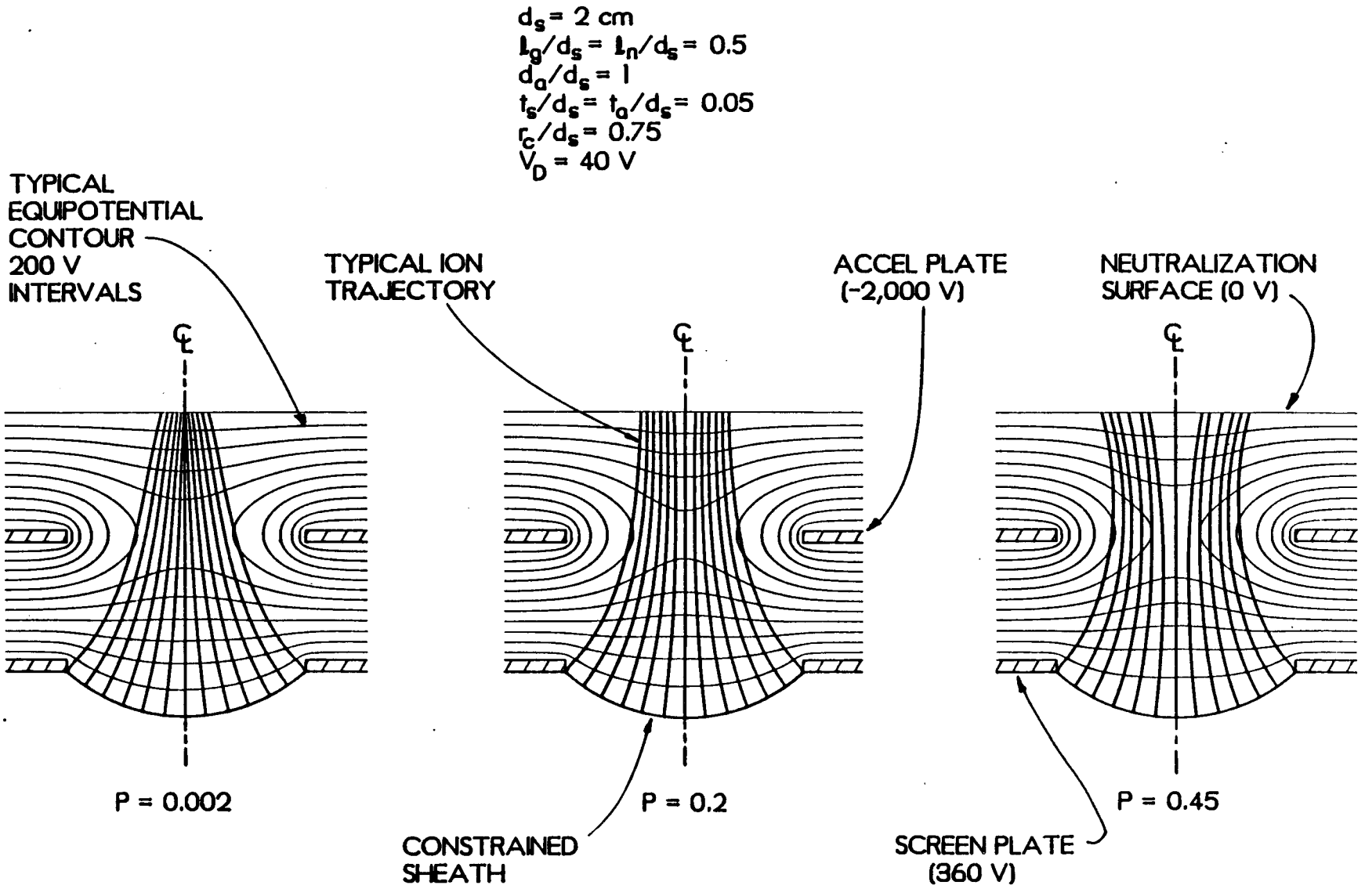


Fig. 4. Beamlet Trajectories through a Single Aperture Constrained-Sheath Optics System Operating at Three Different Perveance Values

surface and the constrained sheath, together with equipotential contours and ion trajectories computed at various perveances for the standard optics system described above, with $r_c/d_s = 0.75$, accel plate voltage $V_a = -2{,}000$ V, screen plate voltage $V_s = 360$ V and discharge voltage $V_D = 40$ V. These correspond to a net ion energy V_N of 400 V and a net-to-total accelerating voltage ratio of 0.167. Ion trajectories through the optics system are depicted by the lines running from the constrained sheath to the neutralization plane and equipotential contour lines run nearly normal to them. For the low perveance case ($P = 0.002$), the ions are seen to have a radially inward-directed component of velocity as they leave the constrained sheath and at this low perveance level the repulsive space-charge induced forces are not strong enough to cause them to turn to the point where they have radially outward-directed velocity components before they reach and cross the neutralization surface. Because the ions feel no net electric field forces in the region downstream of the neutralization surface, they will continue to follow straight line trajectories and will eventually cross the axial centerline and become divergent.

As perveance is increased, a point is reached ($P = 0.2$ case) where the space-charge induced repulsive forces become sufficiently large so that the ion velocities are essentially axial (i.e. with very small radial components). This corresponds to the minimum divergence beamlet for this particular constrained-sheath optics system operating at the discharge plasma and plate operating conditions specified in Fig. 4. Closer examination of the data shows that the outer trajectory ions have small radially inward-directed components of velocity, while ions near the center or the beamlet are traveling

radially-outward. Because of this effect, the beamlet divergence angle is still -4.6° when the beamlet is in its minimum divergence configuration. Since all of the ions will never simultaneously have a zero radial component of velocity when they reach the neutralization surface, there will be no operating condition at which the divergence angle will be zero for the case being considered (double, thin plate optics with a sheath-constraining mesh formed as a spherical segment). It is believed that zero divergence operation could be realized if the sheath shape could be controlled optimally.

As perveance is increased further, the space-charge induced forces also increase until they become sufficiently large so that they cause all of the ions to follow divergent trajectories before they reach the neutralization plane and the beamlet divergence increases from its minimum value. Further increases in perveance induce progressively greater space-charge repulsion effects and corresponding increases in both individual particle and composite beamlet divergence angles. Also shown in Fig. 4 is a case where the perveance has been increased (P = 0.45 case) to the point where all of the ions are repelled from the centerline and arrive at the neutralization surface on divergent trajectories.

Once ion trajectories have been computed, the beamlet current density profile can be found at any location downstream of the neutralization surface and the beamlet divergence angle can be computed. As previously observed, divergence angles computed a finite distance downstream of the accel plate underestimate the true divergence of the beamlet ions; however, if the beamlet current density profile is obtained far downstream of the accel plate, the difference between the actual and computed divergence angles becomes negligible.

Therefore, unless stated otherwise, computer generated divergence angle data given in this report are determined from ion current density profiles computed 800 cm downstream of the accel plate.

Beamlet divergence angles generated as outlined in the preceding paragraphs have been plotted against perveance for the various constrained-sheath geometries identified in Fig. 3 at net-to-total voltage ratios of 0.167, 0.130, 0.091 and 0.048. These particular net-to-total accelerating voltage ratios were selected because the lowest one approaches a value needed in atomic oxygen systems and they illustrate the sensitivity of divergence angle to reductions in net-to-total accelerating voltage ratio.

While conducting this study it was found that beamlets became so divergent under some operating conditions that significant numbers of the ions would be drawn back toward and even strike the accel plate so they could not reach the neutralization surface. When this occurred, the beamlet divergence half angle could have been 90° or greater; however, because the beamlet density profile was determined using data from the current density profile computed 800 cm downstream of the neutralization surface, the divergence angle was always less than 90° and frequently it was as low as 60°. Because of this effect the divergence data over 60° are considered inaccurate and divergence angles greater than this will not be plotted. It is noted in this regard that beamlet divergence angles less than 10° would almost certainly be required in atomic oxygen system applications, so ignoring the inaccurate large divergence angle data does not result in the rejection of any useful data.

A typical plot of computed divergence angle plotted against perveance, for the case where the normalized sheath constraining mesh

radius of curvature is 0.575 and the normalized plate spacing is 0.5, is presented in Fig. 5. Two interesting characteristics that constrained-sheath optics systems exhibit can be seen from the plots in this figure. Namely, there is an optimum perveance at which the beamlet divergence curves go through a minimum and the divergence angle computed at any perveance increases as the net-to-total accelerating voltage ratio is reduced.

The beamlet divergence angle minima shown in the data of Fig. 5 develop because of the trend, pointed out previously, for ions to cross over the axial centerline at low perveances, to follow nearly axial trajectories at higher perveances and to be forced away from the centerline because of ion mutual repulsion forces at still higher perveances. The trend for beamlets to become more divergent as net-to-total accelerating voltage ratio is reduced is also related to ion mutual repulsion (space-charge) effects. Specifically, it reflects the fact that ions extracted through a particular optics system at low net accelerating voltages (low net-to-total accelerating voltage ratios in the present case) travel more slowly through the intraplate region than ions extracted through the same optics system at higher net ion accelerating voltages. As a result the repulsive forces that induce divergence act for longer periods of time and the resultant divergence angles will be greater.

Beamlet divergence data computed for the same optics system dimensions as those in Fig. 5 but for increasingly larger constrained-sheath radii of curvature are shown in Figs. 6-9. An examination of these figures reveals that most of the constrained-sheath configurations studied are unsuitable for producing a low energy, low divergence ion beamlet. In fact, for the deep-dished constraining

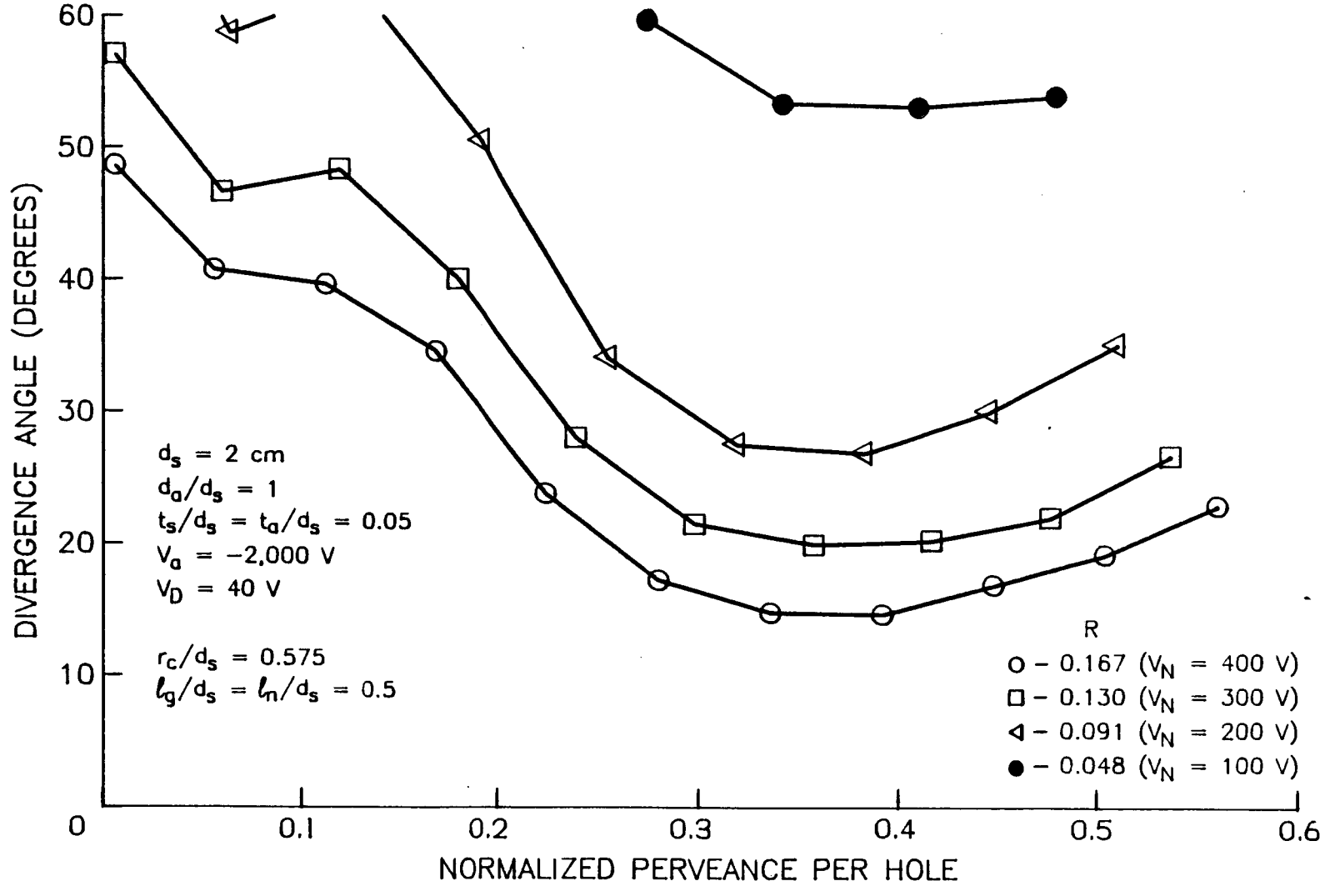


Fig. 5. Computer Generated Divergence Angle Data for r_c/d_s = 0.575 and ℓ_g/d_s = 0.5 Constrained-Sheath Optics System

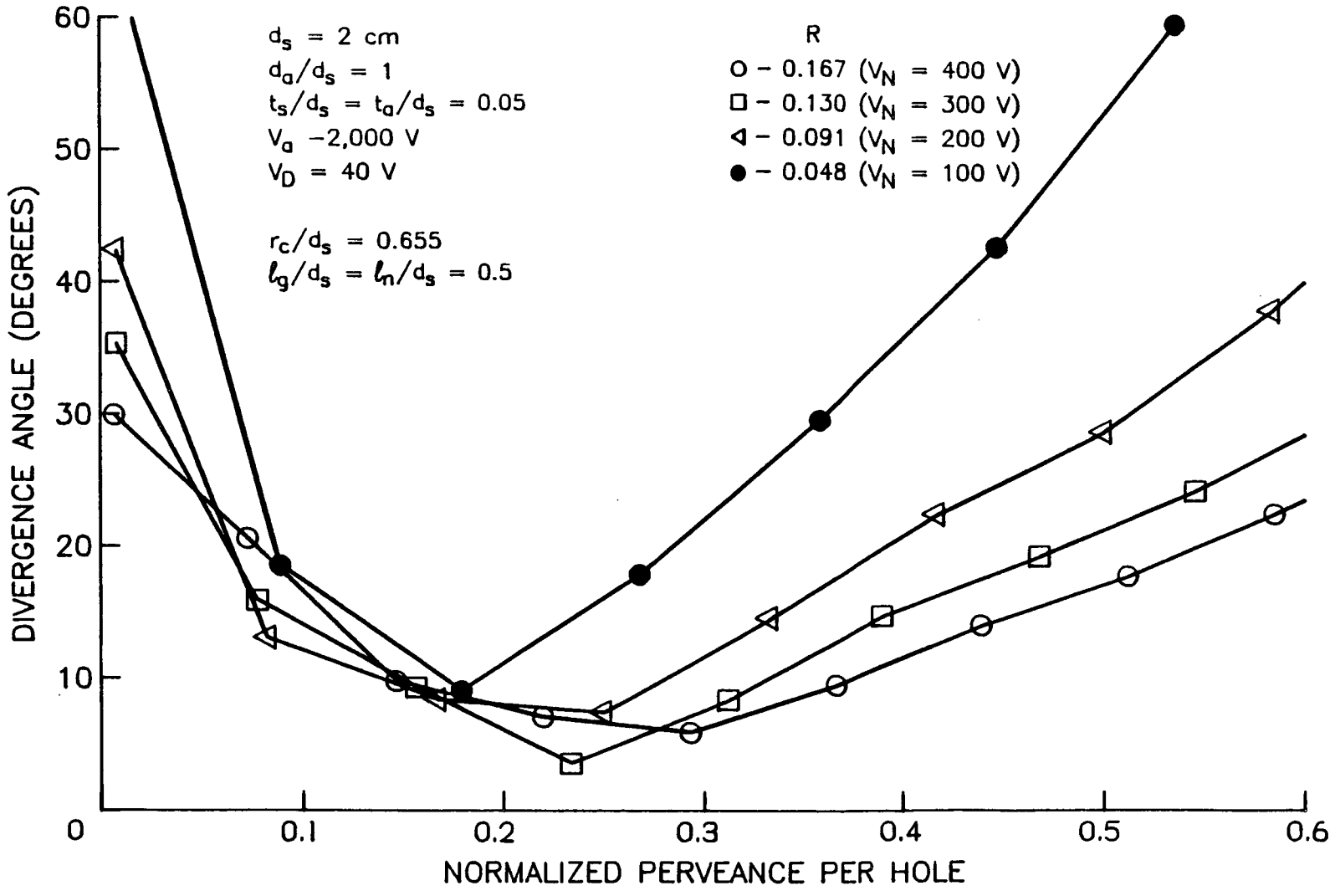


Fig. 6. Computer Generated Divergence Angle Data for r_c/d_s = 0.665 and ℓ_g/d_s = 0.5 Constrained-Sheath Optics System

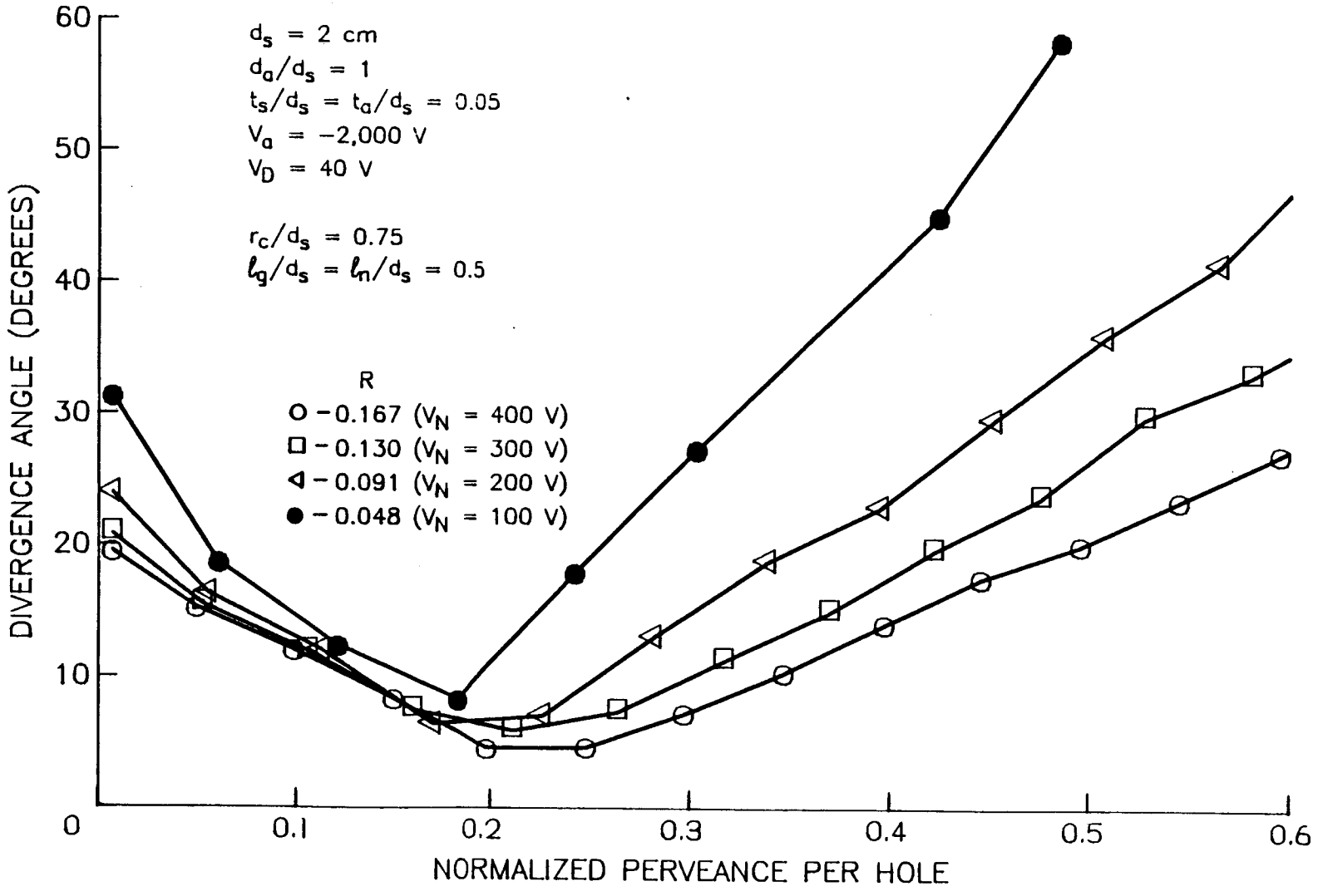


Fig. 7. Computer Generated Divergence Angle Data for r_c/d_s = 0.75 and ℓ_g/d_s = 0.5 Constrained-Sheath Optics System

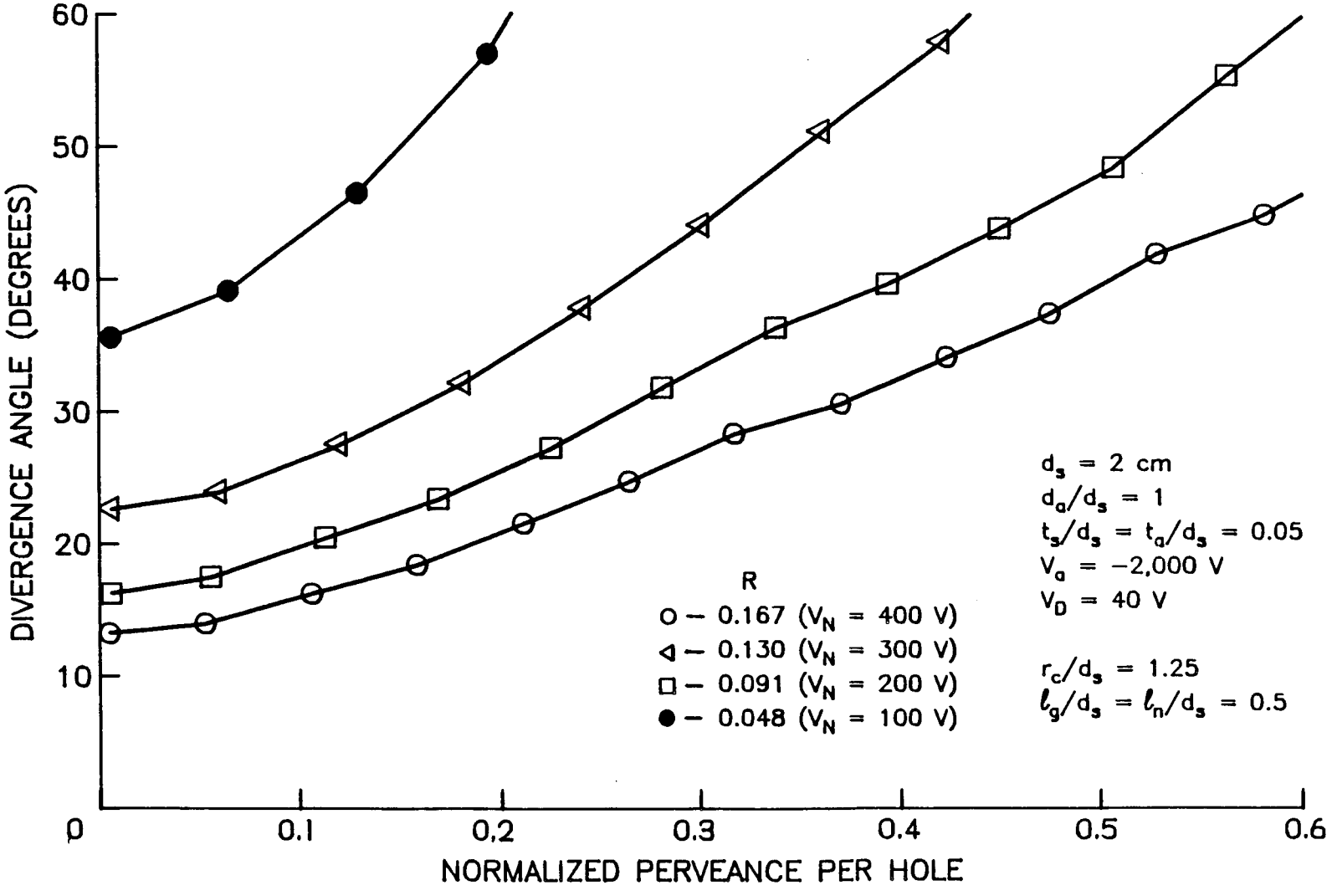


Fig. 8. Computer Generated Divergence Angle Data for r_c/d_s =1.25 and ℓ_g/d_s = 0.5 Constrained-Sheath Optics System

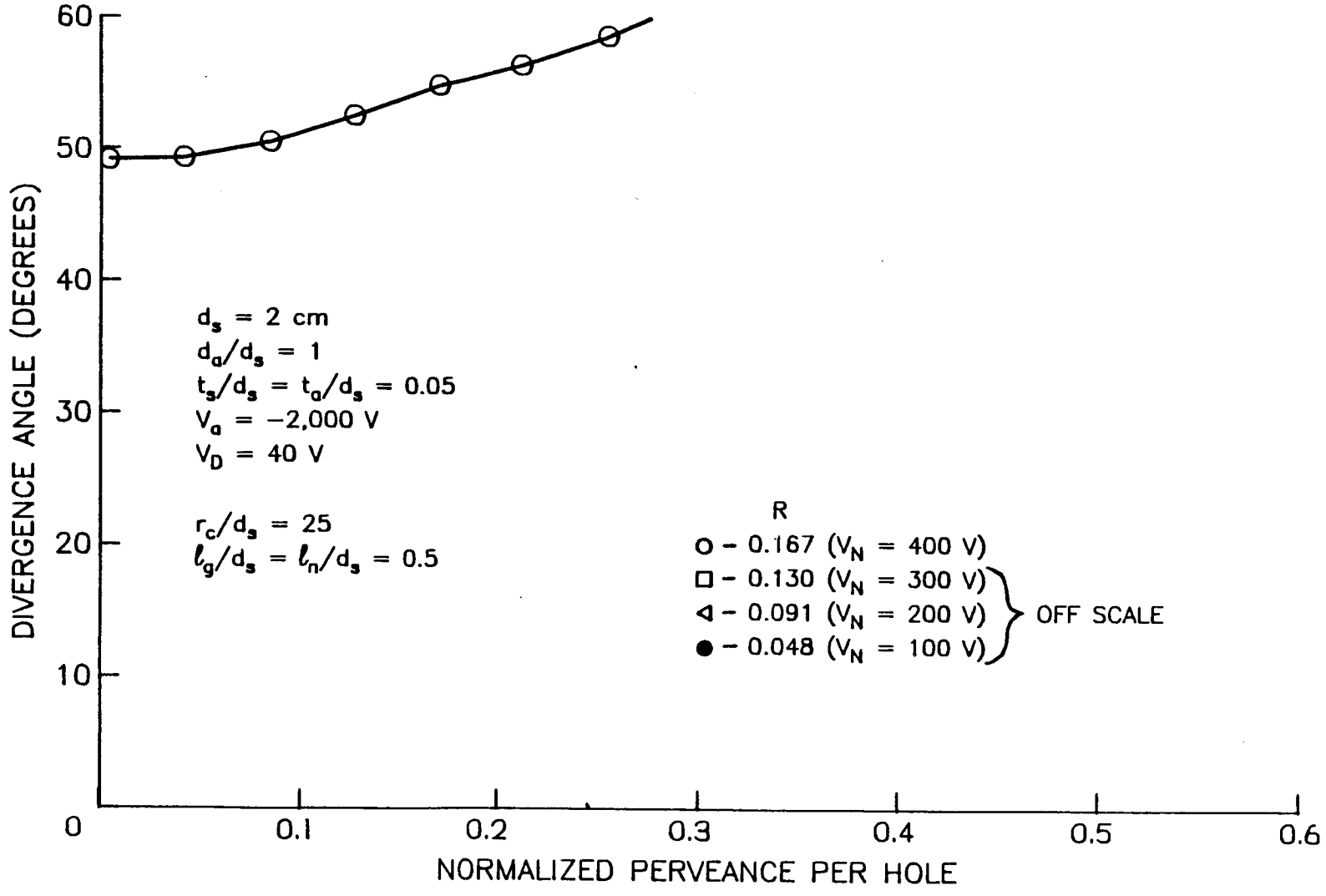


Fig. 9. Computer Generated Divergence Angle Data for r_c/d_s = 25 and ℓ_g/d_s = 0.5 Constrained-Sheath Optics System

sheaths ($r_c/d_s < 0.575$) the data of Fig. 5 and other data not presented here show that the divergence angle for beamlets extracted at a net-to-total accelerating voltage ratio of 0.048 never falls below 50° and for the shallow-dished constraining sheath cases (r_c/d_s = 1.25 and 25) the data of Figs. 8 and 9 show the divergence angle of beamlets with a net-to-total accelerating voltage ratio of 0.048 always exceeds 35°. In general, the maximum acceptable divergence angle is somewhat arbitrarily set at 10° because if the beamlet were more divergent than this it is believed that too much of the ion beam current would be lost on divergent ion trajectories. The two remaining sheath-constraining geometries in this sequence, namely those associated with the data of Figs. 6 and 7, suggest constraining mesh normalized curvatures (r_c/d_s) in the range between ~0.65 and 0.75 could be used to produce the desired low divergence ion beamlets.

Although deep and shallow-dished constrained-sheath geometries are not suitable for producing a low energy, low divergence beamlet, a few comments on the phenomena occurring in these constrained-sheath systems which cause them to have poor divergence characteristics are considered noteworthy. In the deep-dished constrained-sheath optics systems (Fig. 5) there is a large variation in the magnitudes of radially-inward directed velocity components that ions have as they are extracted through the constrained sheath. The magnitude of this velocity is determined by the position on the constrained-sheath surface at which an ion enters the optics system (large radially-inward directed velocity components for ions extracted from positions near the edge of the screen hole and small radial velocity components for ions coming from positions near the aperture centerline). Because of the large variation of the initial radially-inward directed

velocities of the ions entering the optics system, space-charge induced forces cannot simultaneously induce the correct radial velocity change for all of the ions. The result is that the beamlets produced by deep-dished constrained-sheath optics systems exhibit poor divergence characteristics at all net-to-total accelerating voltage ratios and perveances. It is also noted that data collected with very deep-dished constrained-sheaths (r_c/d_s = 0.5 and 0.5125) showed a great deal of data scatter in addition to the large divergence angles. This high degree of scatter is considered to be a consequence of the facts that many of the trajectories cross over each other and that space-charge forces are able to compensate for the initial radial velocities of only a small fraction of the ions being drawn from the constrained-sheath at any given perveance level. Obviously, this effect diminishes as the constrained sheaths become shallower.

The beamlet divergence angle vs. perveance plots for the shallow-dished constrained-sheath optics systems of Figs. 8 and 9 (r_c/d_s = 1.25 and 25) show that the beamlet divergence angle is smallest at zero perveance and that it increases continuously with perveance. This occurs because ions extracted through these optics systems have radially-inward directed velocity components that are small compared to their axial velocity components as they leave the constrained sheath. The radial component of the electric field forces induced by the optics system (excluding space-charge induced forces) are directed radially outward through most of the optics system. Although the radial forces are generally small compared to the forces acting in the axial direction, they do tend to cause the ions to diverge. The result is that very few, if any, ions actually cross over the centerline and most ions have a radially-outward directed velocity

when they reach the neutralization surface. Of course, as perveance increases, space-charge induced forces, which are always directed radially-outward, act to increase the divergence of the ions. These phenomena combine to make shallow-dished constrained-sheath optics systems unsuitable candidates for producing low divergence, low energy ion beamlets.

It is noted that the lowest beamlet divergence angles at low net-to-total accelerating voltage ratios occurred at a perveance level of about 0.2 (Figs. 6 and 7). In order to get a high beamlet current density with reasonably scaled optics systems, it would be desirable to find an optics system geometry where low beamlet divergence angles could be achieved at higher perveances. Changing the screen-accel plate separation distance, ℓ_g, will change the electric field induced by the optics system. To determine if such a change would be beneficial, optics systems in which the normalized plate separation (ℓ_g/d_s) were 0.25 and 1.0 were also investigated. Various constrained sheath radii of curvature for both of these cases and beamlets extracted at net-to-total accelerating voltage ratios of 0.167, 0.130, 0.091, 0.048 were studied.

Figures 10-13 show plots of beamlet divergence angle vs. perveance data for constrained-sheath radii of curvature r_c/d_s of 0.5125, 0.575, 0.75 and 1.25 when the normalized plate separation ℓ_g/d_s was 0.25 and Figs. 14-16 show similar plots generated when ℓ_g/d_s was 1.0 and the normalized curvatures r_c/d_s were 0.575, 0.75 and 1.25.

Consideration of Figs. 10-16 suggests that the same general trends seen in the data when the normalized plate separation was 0.5 (Figs. 5 through 9) are also observed with the larger plates separation ratios. However, somewhat different behavior is observed with the reduced

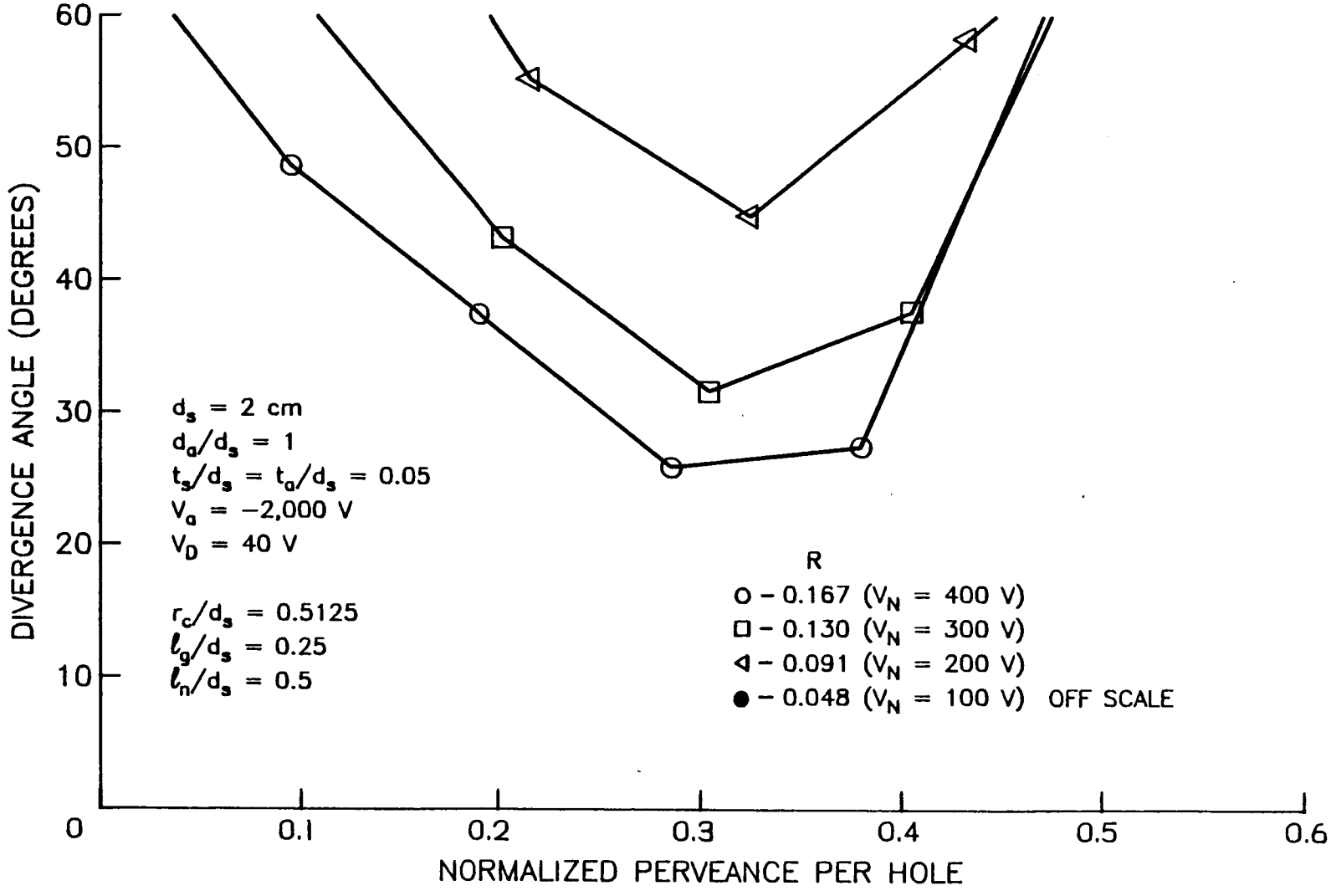


Fig. 10. Computer Generated Divergence Angle Data for r_c/d_s = 0.5125 and ℓ_g/d_s = 0.25 Constrained-Sheath Optics System

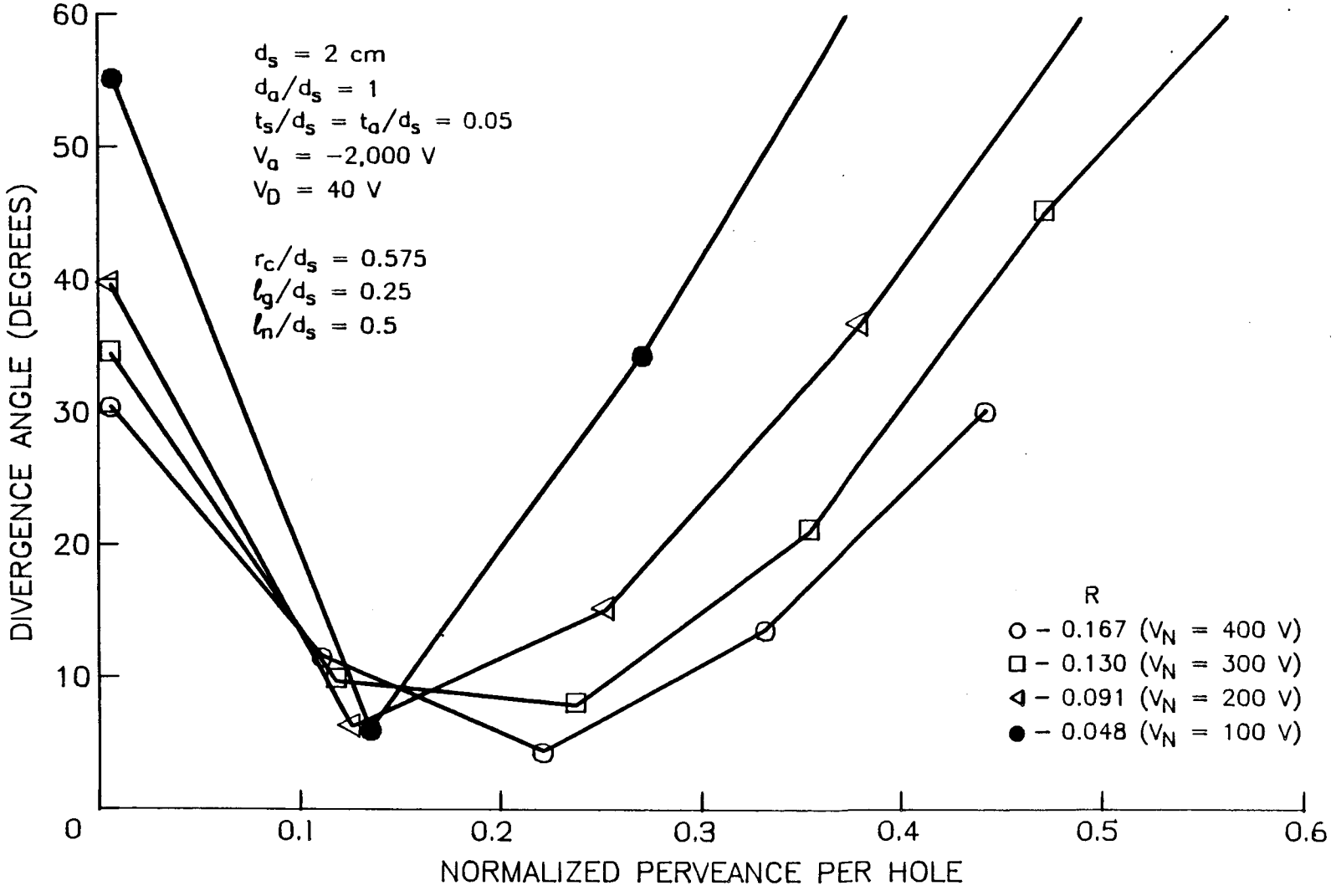


Fig. 11. Computer Generated Divergence Angle Data for r_c/d_s = 0.575 and ℓ_g/d_s = 0.25 Constrained-Sheath Optics System

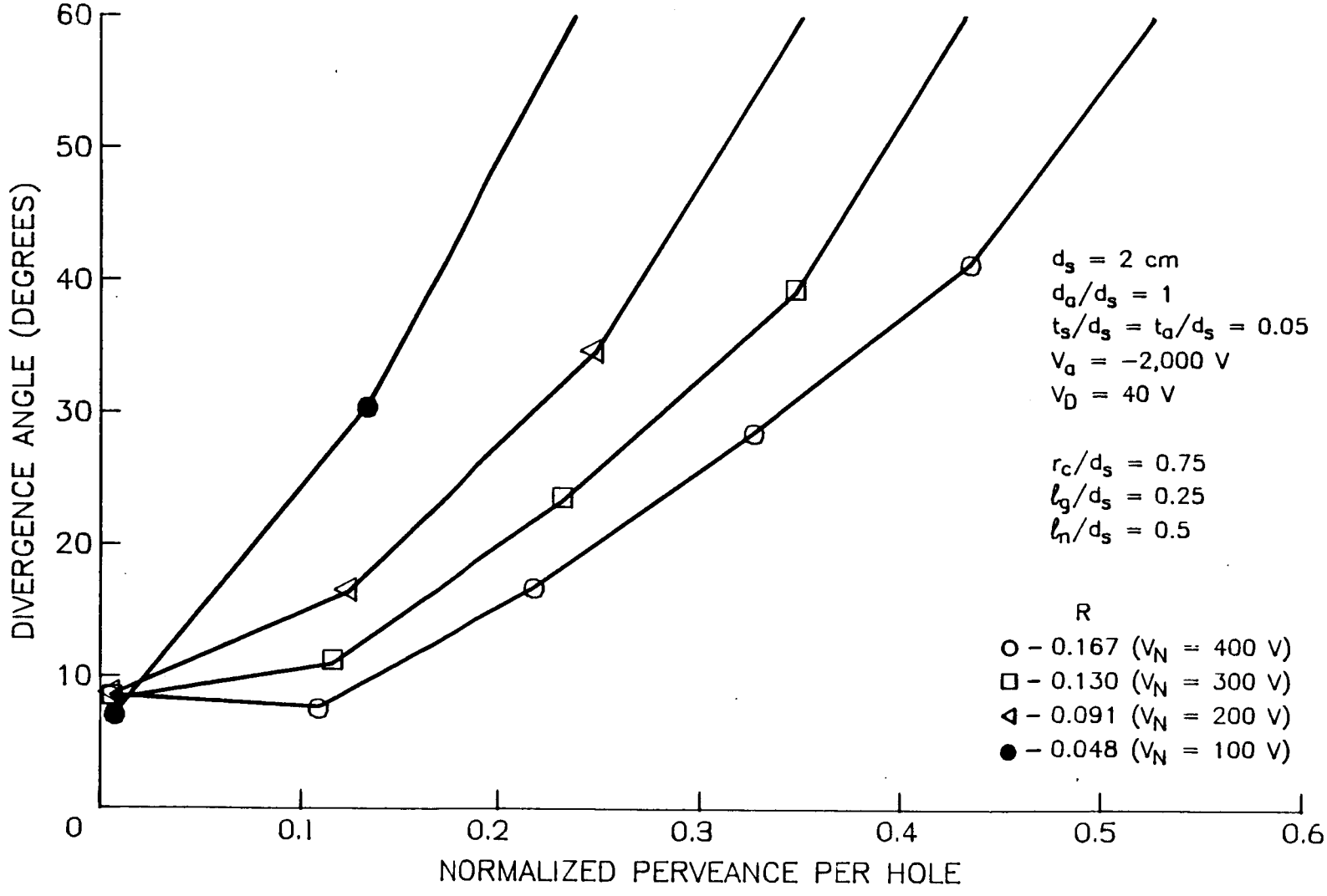


Fig. 12. Computer Generated Divergence Angle Data for r_c/d_s = 0.75 and ℓ_g/d_s = 0.25 Constrained-Sheath Optics System

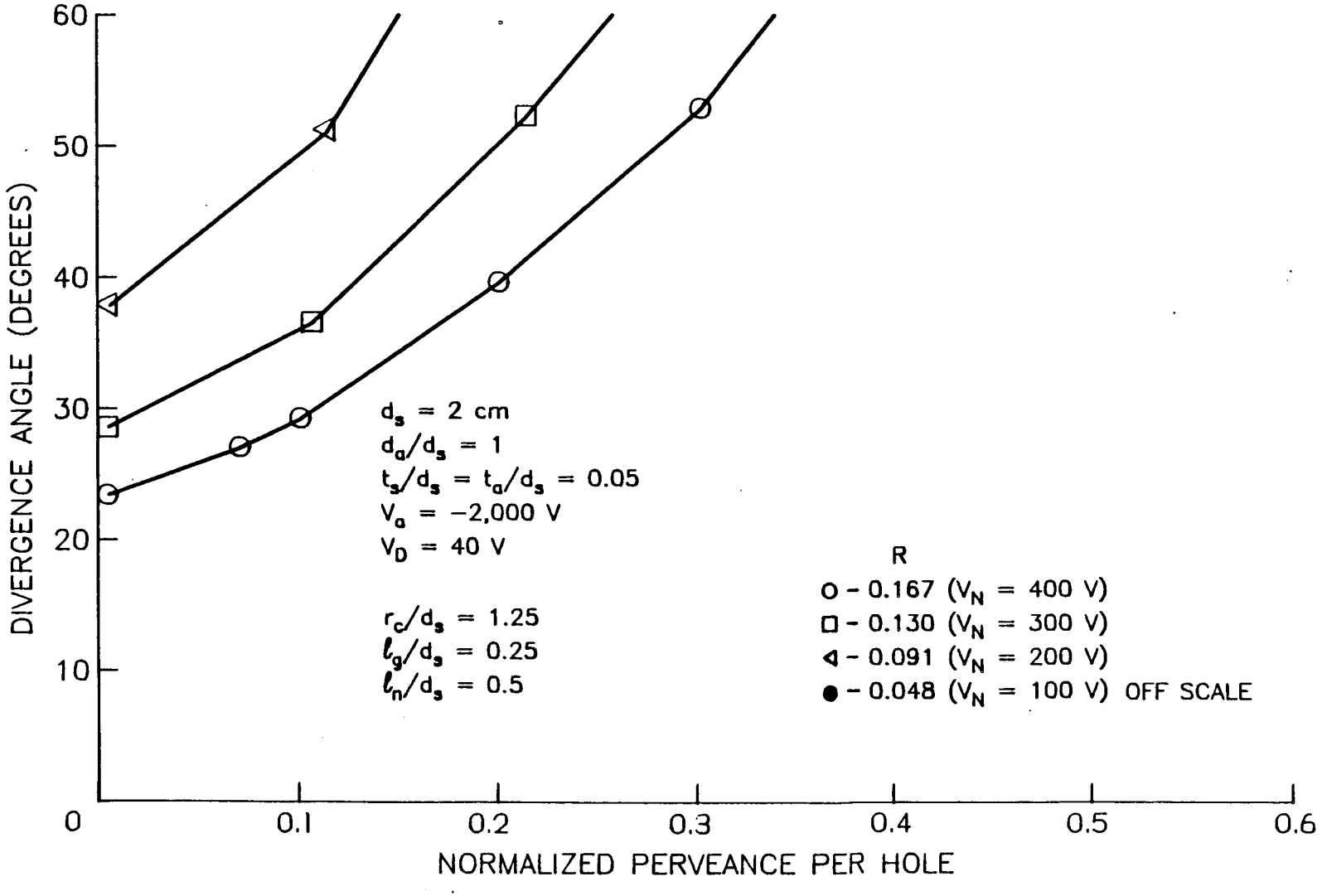


Fig. 13. Computer Generated Divergence Angle Data for r_c/d_s = 1.25 and ℓ_g/d_s = 0.25 Constrained-Sheath Optics System

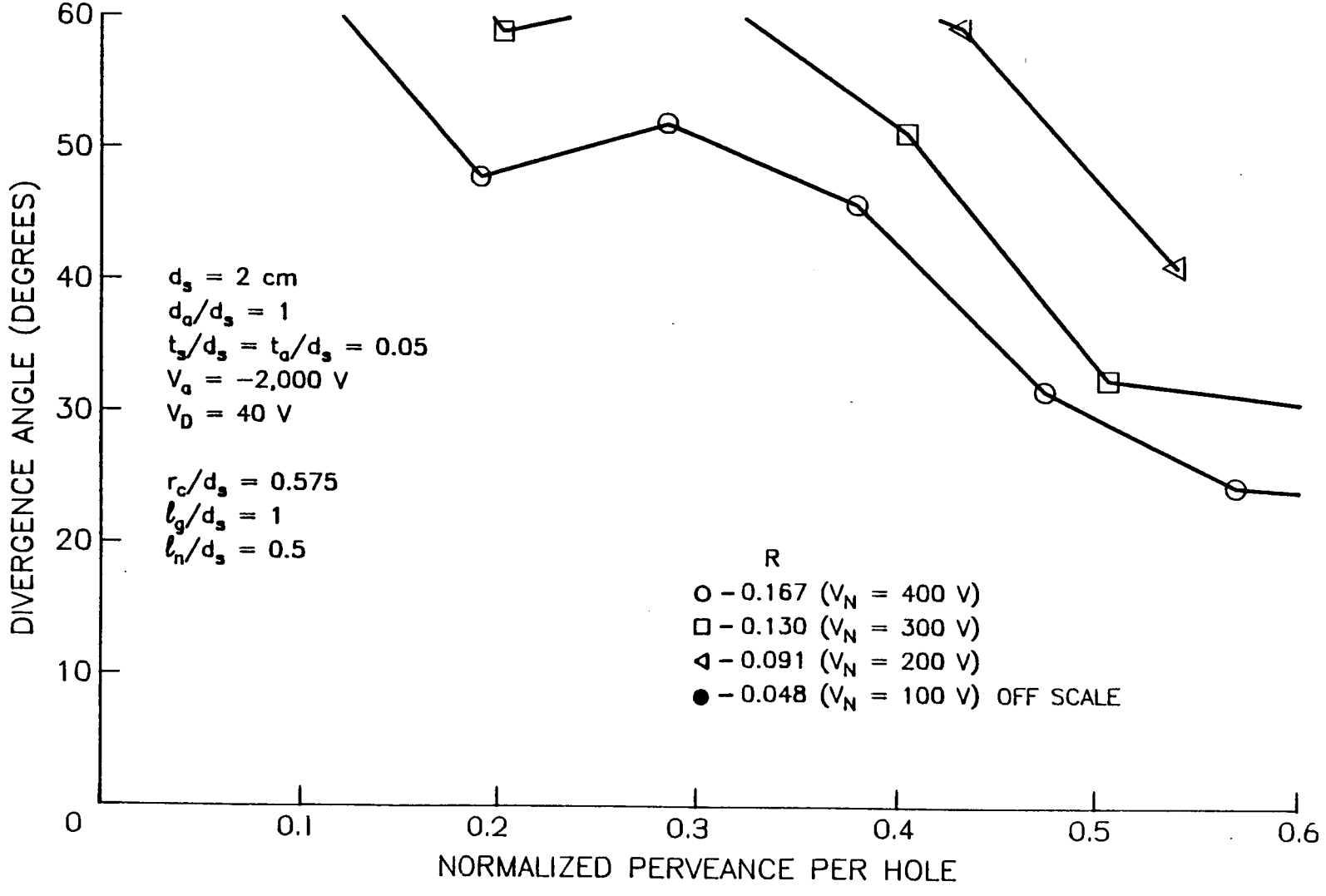


Fig. 14. Computer Generated Divergence Angle Data for r_c/d_s = 0.575 and ℓ_g/d_s = 1 Constrained-Sheath Optics System

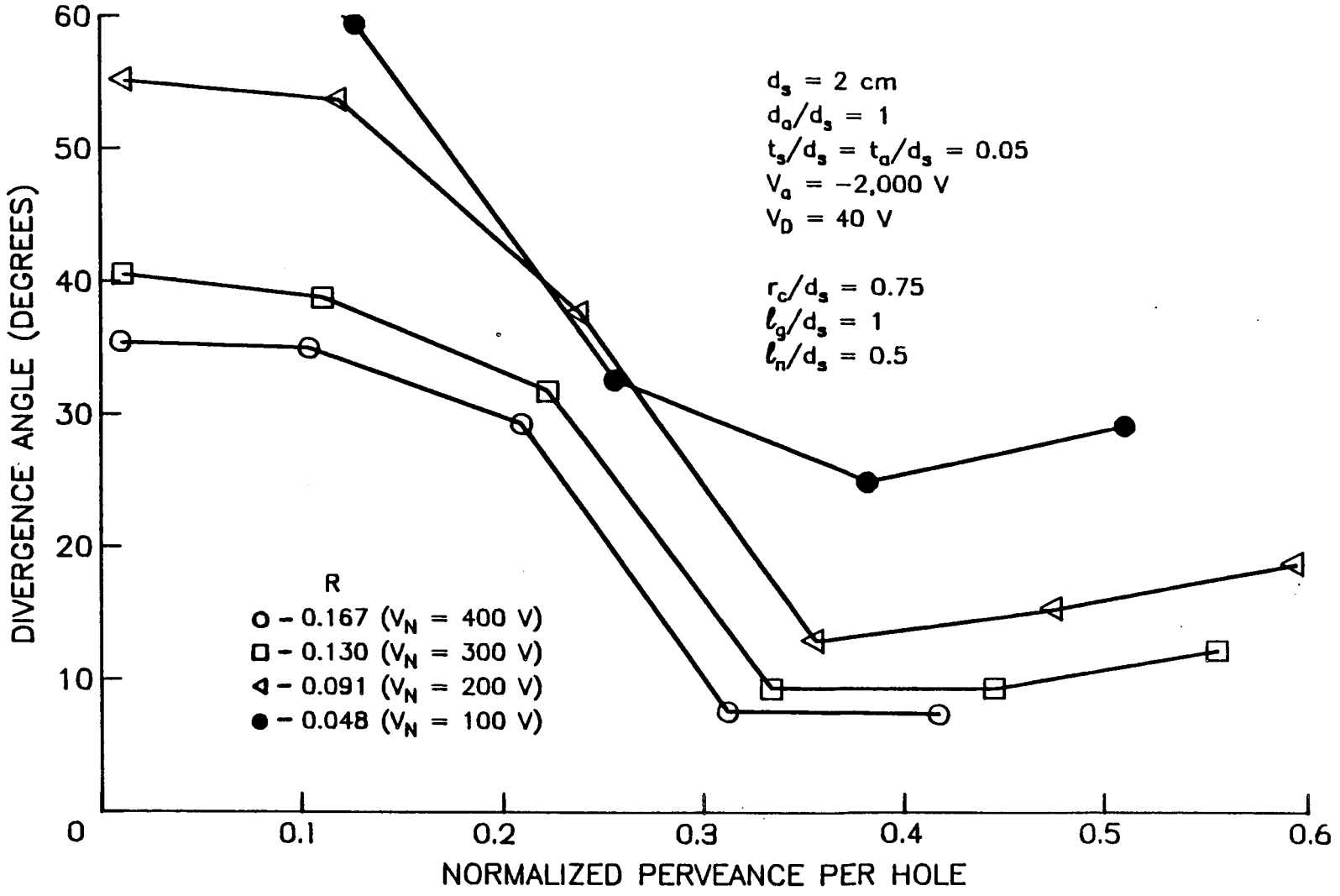


Fig. 15. Computer Generated Divergence Angle Data for r_c/d_s = 0.75 and ℓ_g/d_s = 1 Constrained-Sheath Optics System

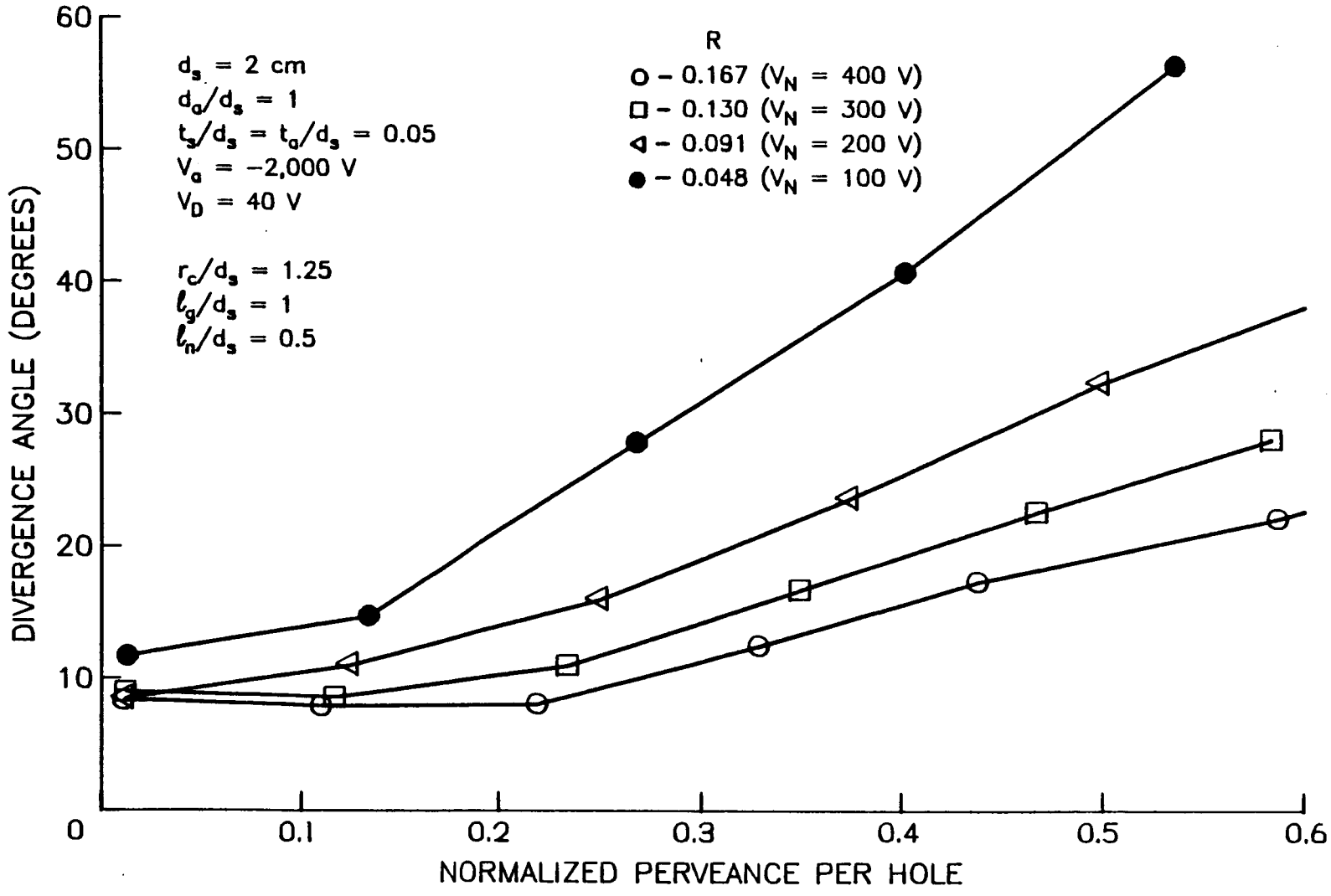


Fig. 16. Computer Generated Divergence Angle Data for r_c/d_s = 1.25 and ℓ_g/d_s = 1 Constrained-Sheath Optics System

plate spacing. In this case the best constrained-sheath optics system has a greater dish depth (r_c/d_s = 0.575) than the best configuration of the optics set with the intermediate spacing (ℓ_g/d_s = 0.5) had. Also, over the range of radii of curvature studied with the large plate spacing (ℓ_g/d_s = 1), the minimum beamlet divergence was obtained with the shallowest dish depth investigated (r_c/d_s = 1.25). It is noted, however, that the optimum constraining-sheath radius of curvature may lie between r_c/d_s = 0.75 and 1.25 for the large plate separation case (ℓ_g/d_s = 1).

In spite of the fact that the radius of curvature at which minimum beamlet divergence occurs changes with plate separation, the data indicate that the perveance level at which the minimum occurs is still low (about 0.2) so changing the plate spacing does not facilitate operation at high current density levels.

OPTICS SYSTEM SCALING EXAMPLE

An example of how to scale an optics system to obtain a beamlet with the same divergence angle, but with a different ion energy and beamlet current density, as that of a known optics system will be given here. The example will be taken from the data shown in Fig. 6. The point on the curve where the net-to-total accelerating voltage ratio is 0.048, the perveance is 0.18 and the beamlet divergence angle is 9° was chosen. The beam current density at the constrained sheath is given at a prescribed operating condition in terms of the beam current per hole (J_B) by

$$j = \frac{J_B}{A} \tag{8}$$

where A is the area of the sheath constraining mesh given by

$$A = 2\pi r_c^2 \left[1 - \cos\left(\sin^{-1} \frac{d_s}{2r_c}\right)\right] \quad . \tag{9}$$

One other variable needed to find J_B in Eq. 3 is the effective accelerating length (ℓ_e) given by

$$\ell_e = \ell_g + t_s + r_c\left[1 - \cos\left(\sin^{-1} \frac{d_s}{2r_c}\right)\right] \quad . \tag{10}$$

Using Eqs. 3, 8, 9 and 10 together with the dimensions given on Fig. 6 and the mass and charge of a singly ionized argon atom, the beamlet current density j associated with the numerical calculations that produced the Fig. 6 results is found to be 0.05 mA/cm^2.

For the 5 eV atomic oxygen source on the other hand, the desired operating condition might be $V_N = 5$ V and $j = 0.2$ mA/cm^2. Using these requirements in Eqs. 3, 4, 8, 9, and 10 yields a requirement that the screen hole diameter be 1.3 mm and the total accelerating voltage be 104 V at the required perveance of 0.18. Since all the optics system dimensions must scale down by 1.3/20 = 0.067, the screen and accel plates would be unreasonably thin in this case; however, the other dimensions would be reasonable. The desired optics system could be made larger by operating at a lower net-to-total accelerating voltage ratio; however, this would cause the beamlet divergence angle to

increase. If the plate thicknesses were increased, the relative geometry of the optics system would change and this would probably cause an increase in beamlet divergence.

This example illustrates the difficulties that arise when a low energy, low divergence, high current density ion beamlet is desired; however, the fact that the divergence angle vs. perveance curves go through a minimum at low divergence angles even when the net-to-total accelerating voltage ratio is small indicates that it should be possible to build an optics system capable of producing a low net energy, high current density ion beamlet with reasonably low divergence characteristics.

COMPARATIVE EXPERIMENTAL STUDY

Using the results obtained from the preceding numerical study as a guide, a preliminary experiment was conducted using the constrained-sheath geometry and operating conditions identified as promising from the data in Fig. 6. The results of this experiment as well as some of the problems identified during the test and the comparison of the numerically predicted results with those obtained experimentally are discussed in the following sections of the report.

Experimental Apparatus

The experimental apparatus used to study the constrained-sheath optics concept is shown schematically in Fig. 17. The discharge chamber was equipped with a single aperture pair, constrained-sheath optics set and Fig. 17 shows this plate system along with a conceptualized ion beamlet that might be extracted from it. The

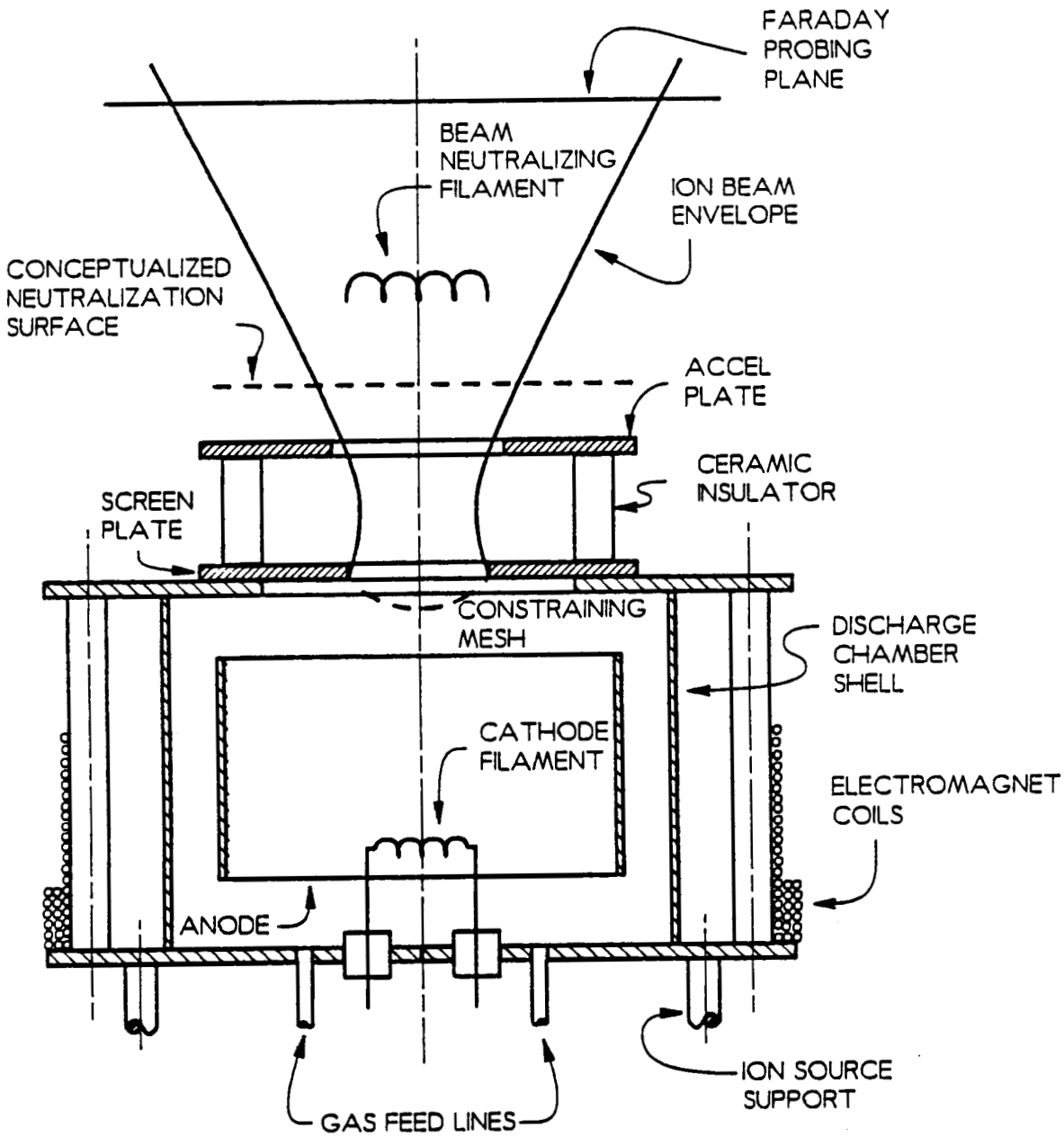


Fig. 17. Discharge Chamber and Optics System

system utilizes a mildly divergent magnetic field discharge chamber which can be operated on a variety of gases. The large diameter single beamlet shown being extracted through the screen and accel plates, which are separated by a relatively large distance, was selected so that the detailed structure of the ion beamlet could be studied. As indicated previously, in an actual application on an atomic oxygen source both the hole size and the plate separation distance would be scaled down to produce higher current density beamlets that those obtainable in this device.

As Fig. 17 suggests, a Faraday probe was used to measure beamlet current density profiles downstream of the accel plate and this probe is shown in Fig. 18. The basic mechanical elements of this system include a drive rod attached to a support arm which holds the Faraday probe sensor assembly and a position-sensing potentiometer. When the drive rod and support arm are rotated, the sensor assembly sweeps through the ion beamlet being studied. As Fig. 18 suggests, the ion beamlet current density is sensed by allowing a small portion of the beamlet to strike a molybdenum plate after passing through a 2 mm diameter aperture. The electron current that must flow to the plate to neutralize this collected ion current induces a voltage drop across the 1000 ohm resistor shown and this provides a signal to the Y channel of the X-Y recorder. The Faraday probe radial position relative to the ion beamlet centerline is sensed by the potentiometer shown attached to the end of the drive rod in Fig. 18 and this signal is sent to the X channel of the recorder. In order to prevent plasma electrons from reaching the molybdenum plate, the entire probing assembly is held at a potential 5 V negative of ground. The grounding screen shown on the downstream side of the probe assembly in Fig. 18

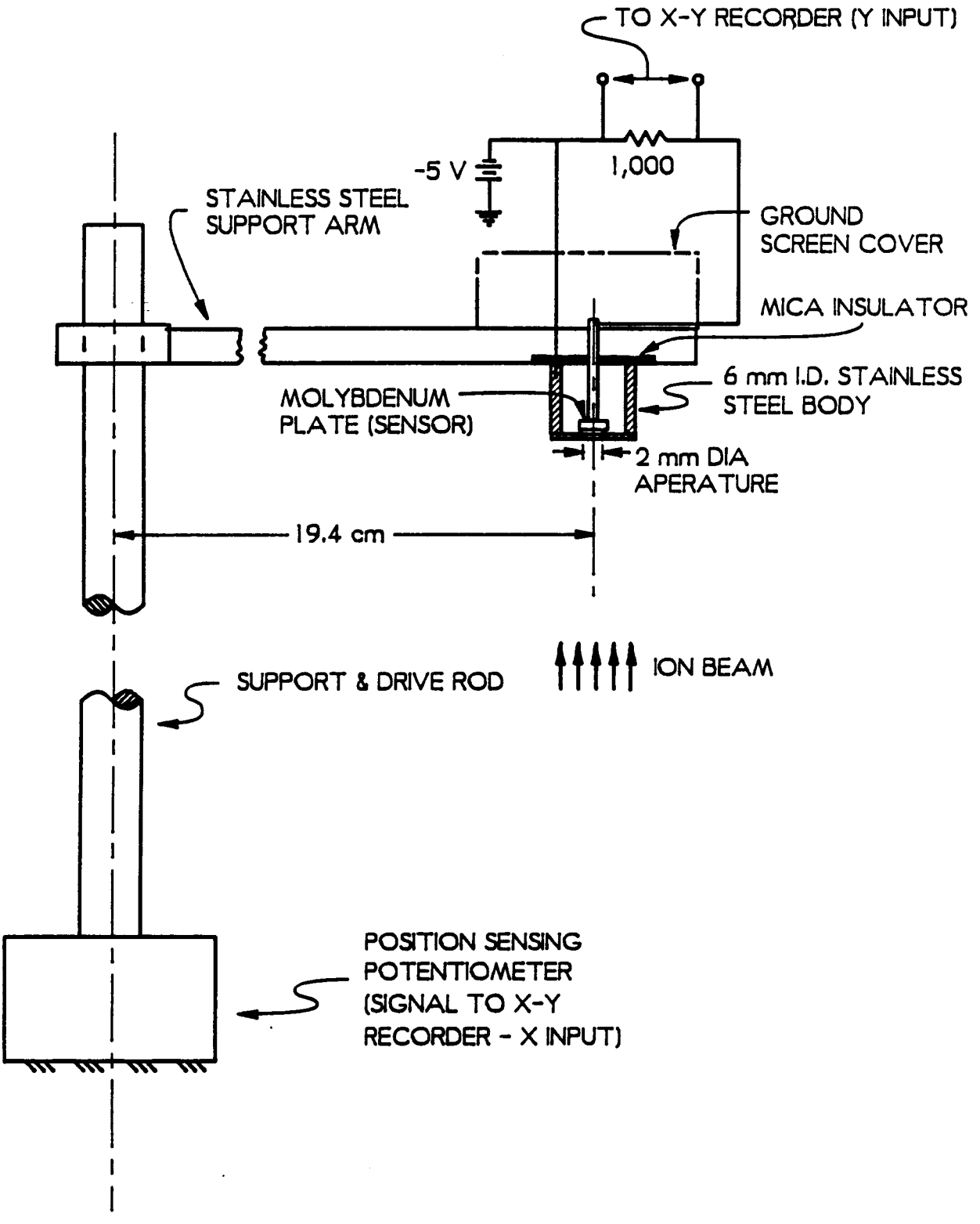


Fig. 18. Faraday Probe

serves to isolate connections to the probe from the beamlet plasma; this prevents stray currents from being collected and sensed.

Preliminary Experimental Results

A preliminary experiment was conducted to test the constrained-sheath optics system that corresponded to the beamlet divergence angle vs. perveance data shown in Fig. 6. This system was a two-plate single aperture constrained-sheath optics system with d_s = 2.9 cm, ℓ_g/d_s = 0.5, d_a/d_s = 1, t_s/d_s = t_a/d_s = 0.05, r_c/d_s = 0.655, which was operated with V_a = -2,000 V, V_s = 360 V, V_D = 40 V and a net-to-total accelerating voltage ratio of 0.17. In order to measure the ion beamlet current density profiles from which divergence angle data could be computed, the Faraday probe was located 12 cm downstream of the accel plate. These current density profiles were subsequently integrated and the radial location which enclosed 95% of the beamlet current was found and converted into beamlet divergence data. Total integrated beamlet currents were found to agree with those measured directly to within 10% except at perveance levels below 0.1 where the integrated currents underestimated the measured currents by up to 40%; this is attributed to a loss of probe sensitivity at low current levels. Also, when the beamlet divergence exceeded about 30° the integrated beamlet currents underestimated the measured ones by up to 25% and it is believed that this effect might reflect an inability of the probe to collect ions on highly divergent trajectories.

In order to compare the experimental results with the computer predictions, the computer program was used to compute beamlet current density profiles 12 cm downstream of the accel plate. As noted previously, beamlet divergence angles based on beamlet current density

profiles measured near the accel plate will be less than the true values, but the Faraday probe could not be located further away from the accel plate in these tests because of physical constraints imposed by the experimental apparatus. The computer-generated beamlet divergence angles based on current density profiles computed 12 cm downstream of the accel plate were found to be about 5° less than the true divergence angles (i.e. those based on profiles computed at a location 800 cm downstream of the accel plate and shown in Fig. 6) at all perveance levels. Although the divergence angles computed from the current density profiles obtained 12 cm from the accel plate may be low, it would be reasonable to conclude that the true beamlet divergence angles are those given in Fig. 6, if it could be shown that the experimental and computer-generated data agree.

Figure 19 presents plots of beamlet divergence angle vs. perveance obtained from the experimental data (circles) and also from the computer program (squares). Comparison of these curves shows that there is a substantial difference between the experimental and computer-generated data. A possible reason for this discrepancy is that the computer program development was based on the assumption that the ions are traveling perpendicular to the constrained-sheath surface when they enter the acceleration region. It is suggested that this might be a reasonable assumption at low discharge chamber plasma densities (low perveances where the two curves come closer to each other) but it might not be a good assumption at high discharge chamber plasma densities. In fact the constraining-sheath wire mesh might "look" like a solid surface to ions when plasma densities are low and Debye lengths are large; in this case the sheath might appear to be everywhere parallel to the wire mesh. Such an ideal sheath is shown

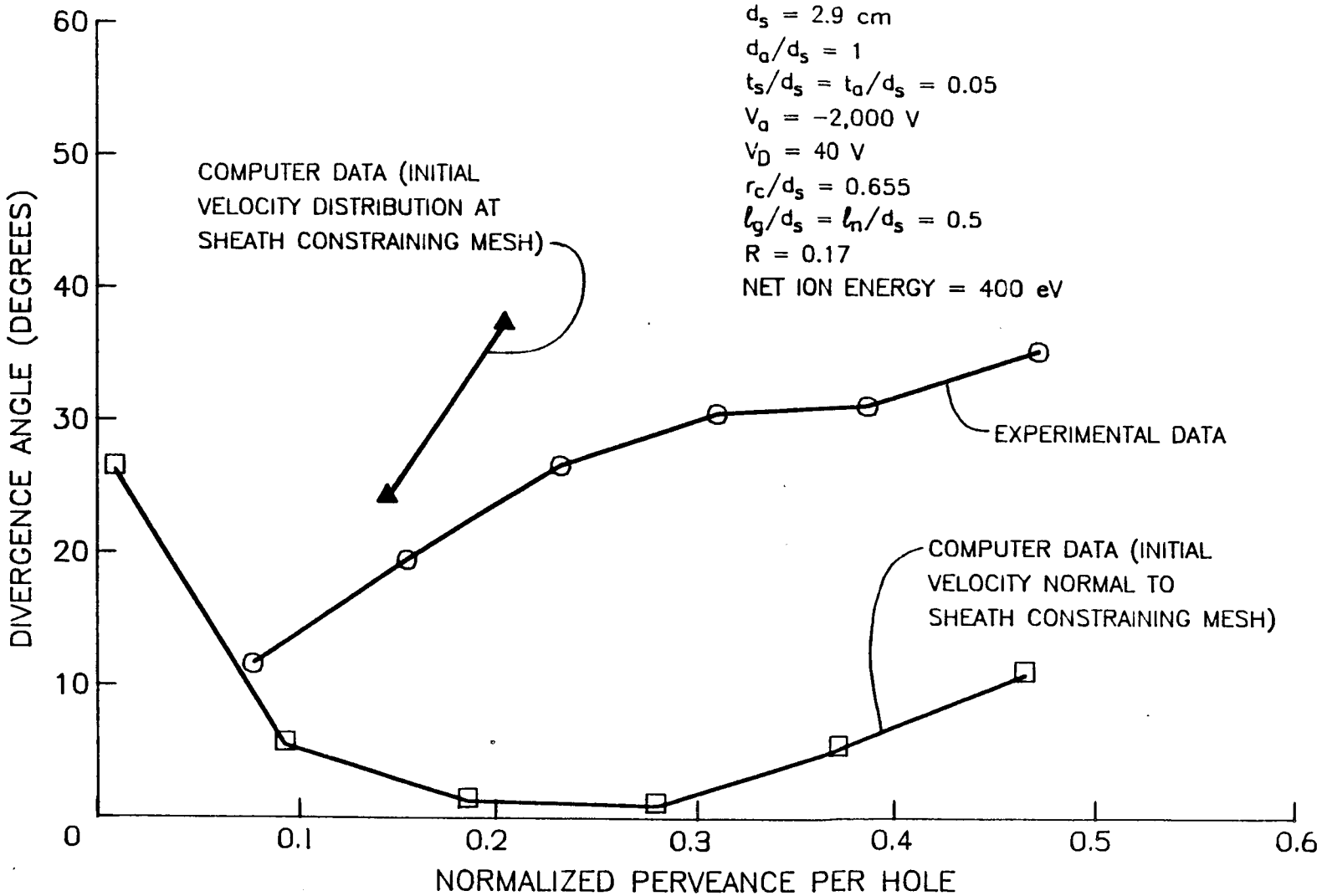


Fig. 19. Comparison of Experimental and Computer Generated Divergence Angle Data for Constrained-Sheath Optics System

in the upper sketch of Fig. 20 (labeled "Low Plasma Density") which shows a cross-sectional view of the screen plate hole and the sheath constraining wire mesh. The ideal sheath which might form at low plasma densities is shown parallel to both the screen plate surface and the contoured wire mesh. Also shown are arrows crossing the sheath and passing through the spaces between the wire mesh; these represent the trajectories of ions leaving the plasma and entering the optics system. Ions cross the sheath at the Bohm velocity which is perpendicular to the sheath and the assumption used in the computer program was that this was also perpendicular to the constraining-sheath wire mesh.

The lower sketch in Fig. 20 (labeled "High Plasma Density") suggests how the sheath might appear at high discharge chamber plasma densities (corresponding to high perveance levels) where Debye lengths would be small. In this situation electrons might begin to travel through the holes between the wires before being turned back by the adverse electric field in the ion acceleration region between the plates. As a result, the sheath could bulge into the gap between adjacent wires in the manner suggest in this sketch. Because the ions would still be on trajectories normal to the sheath at the points where they crossed its surface they would, in this situation, find themselves moving with initial velocities that were not perpendicular to the mean contour of the sheath constraining wire mesh. Rather, they would have the distribution of angles with respect to the mean surface contour suggested by the arrows in this figure.

In order to determine if such a distribution of angles might cause beamlet divergence to increase, the computer program was modified so

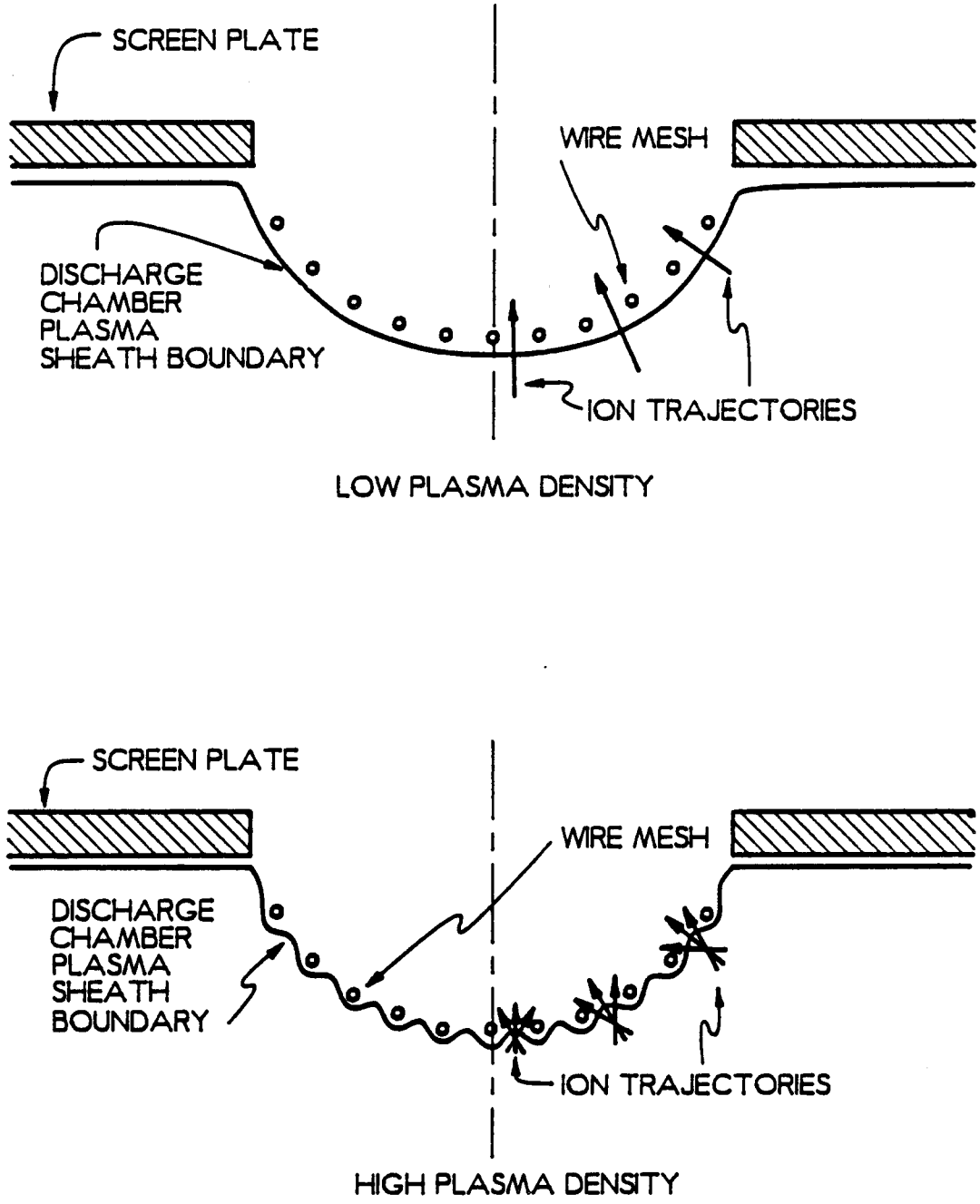
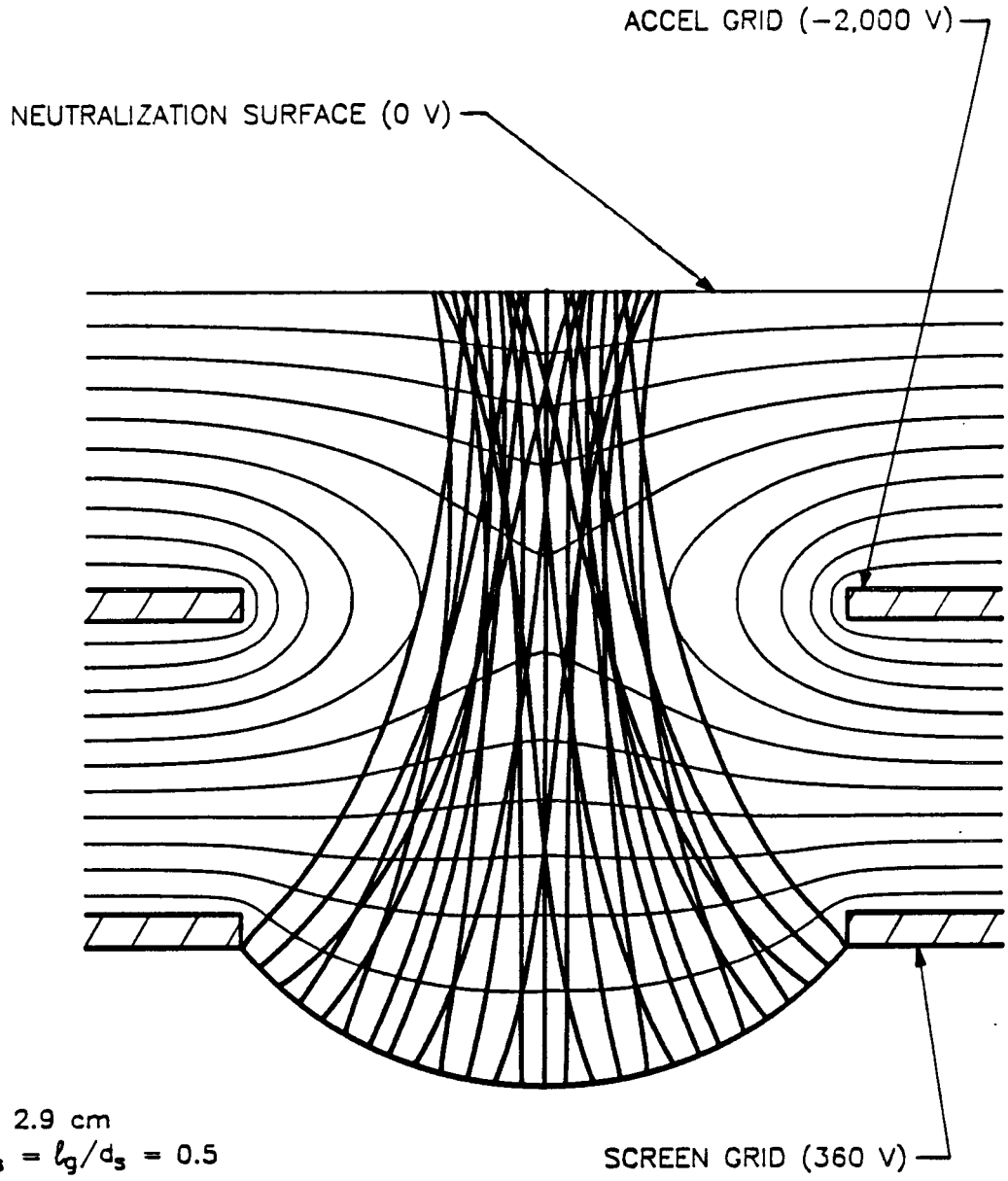


Fig. 20. Variation in Initial Ion Velocity and Sheath Boundary Geometry at High and Low Plasma Densities

that the trajectories of ions having a distribution of non-perpendicular velocities at the constraining-sheath wire mesh could be computed. In reality, this is a three-dimensional problem because the ions can have axial, radial and azimuthal components of velocity as they enter the optics system; however, the sheath shape is not known and therefore neither are the various components of ion velocity as they enter the optics system. Since these angles are not known, they were arbitrarily chosen so that the computer simulation could be conducted. The azimuthal component of velocity was chosen to be zero (otherwise the computer program would have required extensive revision) and the radial and axial components of initial ion velocity were chosen such that the ions had a distribution of angles within ±15° of the perpendicular to the sheath-constraining wire mesh contour. Figure 21 shows beamlet trajectories generated when this initial velocity boundary condition was applied. It is noteworthy that many of the ions are traveling on divergent trajectories when they arrive at the neutralization surface. When the beamlet divergence angles associated with trajectories like those in Fig. 21 are computed they are, as a result, greater than those generated by applying the "normal-to-mesh contour" velocity boundary condition. Divergence angles associated with beamlets having an angular spread in their initial velocities have been computed at two perveance levels and they are shown as the two shaded triangular data points in Fig. 19. Comparison of these data with points on the curves associated with the square symbols indicates the extent of the change in divergence angle induced be changing the angular velocity distribution from ±15° to zero.



d_s = 2.9 cm
$\ell_g/d_s = \ell_g/d_s$ = 0.5
d_a/d_s = 1
$t_s/d_s = t_a/d_s$ = 0.05
r_c/d_s = 0.655
V_D = 40 V
P = 0.23

Fig. 21. Beamlet Trajectories with Initial Velocity Distribution through a Constrained Sheath Optics System Operating at 0.23 Normalized Perveance Per Hole

Given that the initial ion velocity spread of ±15° was arbitrarily assumed, the shaded triangular data points in Fig. 19 cannot be expected to coincide with the experimental data; however, if the suggestion that a distribution of angles at the constraining-sheath wire mesh causes beamlet divergence to increase is correct, the shaded triangle data points should follow the same general trend as the experimental data. As seen on Fig. 19, the shaded triangular computer generated data points do follow the experimental trend qualitatively and this suggests that the constraining-sheath wire mesh influences the discharge chamber plasma sheath geometry and thereby determines the beamlet divergence behavior. The spacing between wires in the constrained-sheath mesh used in the experiment was ~1.5 mm. A more closely spaced and finer wire mesh would probably reduce the divergence angle by causing the sheath that forms at the holes between the wires to approach the ideal shape shown in the upper sketch of Fig. 20. More work needs to be done to determine what the optimum constraining-sheath wire mesh size should be.

CONCLUSIONS

A computer program has been developed to model the extraction of a single beamlet through a two-plate, single aperture pair constrained-sheath optics system. The program has been used to study the divergence characteristics of low energy beamlets for use in a 5 eV atomic oxygen source. This theoretical study indicates that it should be possible to extract a low energy, low divergence ion beam from a constrained-sheath optics system. An experiment conducted to verify this did not correlate well with the computer generated data. It is

thought that the discrepancy exists because a coarse wire mesh was used to constrain the sheath in the experiment. A fine wire mesh should reduce beamlet divergence and give better agreement between experiment and theory. Experiments to verify this have not been conducted; however, it appears that extracting a low energy, low divergence beamlet should be possible at low perveance levels.

REFERENCES

1. Leger, L. J. and Visentine, J. T., "Protecting Spacecraft from Atomic Oxygen", Aerospace America, July 1986, pp. 32-35.

2. Zimcik, D. G. and Maag, C. R., "Results of Apparent Atomic Oxygen Reactions with Spacecraft Materials During Shuttle Flight STS-41G", Journal of Spacecraft and Rockets, March-April 1988, pp. 162-168.

3. Wilbur, P. J. and Han, J. Z., "Constrained-Sheath Optics for High Thrust-Density, Low Specific-Impulse Ion Thrusters", AIAA Paper No. 87-1073, May 1987.

4. Brewer G. R., Ion Propulsion, Gordon and Breach Science Publishers, Inc., New York, 1970, p. 168.

5. Hazma V. and Richley E. A., "Numerical Solution of Two-Dimensional Poisson Equation: Theory and Application to Electrostatic-Ion-Engine Analysis", NASA Tech. Note TN D-1323, October 1962.

6. Bogart, C. D. and Richley, E. A., "A Space-Charge-Flow Computer Program", NASA Tech. Note TN D-3394, April 1966.

DISTRIBUTION LIST

	Copies
National Aeronautics and Space Administration Washington, DC 20546 Attn:	
RP/Mr. Earl E. VanLaningham, MS B600	1
RP/Mr. Robert A. Wasel, MS B600	1
MT/Mr. Edward J. Brazill, MS B326	1
National Aeronautics and Space Administration Lewis Research Center 21000 Brookpark Road Cleveland, OH 44135 Attn:	
Technology Utilization Office, MS 7-3	1
Report Control Office, MS 60-1	1
Library, MS 60-3	2
Dr. M. Goldstein, Chief Scientist, MS 5-9	1
Mr. Dave Byers, MS 500-219	1
Mr. Vince Rawlin, MS 500-220	1
Mr. Bruce Banks, MS 302-1	2
Mr. Mike Mirtich, MS 302-1	1
Ms. Sharon Rutledge, MS 302-1	2
Mr. Michael Patterson, M.S. 500-220	1
National Aeronautics and Space Administration Lyndon B. Johnson Space Center Houston, TX 77058 Attn:	
Dr. James E. McCoy, Code SN3	1
National Aeronautics and Space Administration Marshall Space Flight Center Huntsville, AL 35812 Attn:	
Mr. Robert Bechtel	1
Mr. Ralph Carruth	1
Mr. Jason Vaughn	1
NASA Scientific and Technical Information Facility P.O. Box 8757 Baltimore, MD 21240 Attn:	
Accessioning Dept.	1

	Copies
Dept. of the Navy Office of Naval Research University of New Mexico Bandolier Hall West Albuquerque, NM 87131 Attn:	
G. Max Irving	1
Case Western Reserve University 10900 Euclid Avenue Cleveland, OH 44106 Attn:	
Dr. Eli Reshotko	1
Air Force Astronautics Lab Edwards AFB, CA 93523 Attn:	
LKDH/Lt. Robert D. Meya, MS 24	1
LKDH/Lt. Phil Roberts, MS 24	1
Jet Propulsion Laboratory 4800 Oak Grove Laboratory Pasadena, CA 91102 Attn:	
Technical Library	1
Mr. James Graf	1
Dr. Dennis Fitzgerald	1
Dr. Dave King	1
TRW Inc. TRW Systems One Space Park Redondo Beach, CA 90278 Attn:	
Mr. Sid Zafran	1
National Aeronautics and Space Administration Ames Research Center Moffett Field, CA 94035 Attn:	
Technical Library	1
National Aeronautics and Space Administration Langley Research Center Langley Field Station Hampton, VA 23365 Attn:	
Technical Library	1

	Copies
Hughes Research Laboratories 3011 Malibu Canyon Road Malibu, CA 90265 Attn:	
Mr. J. H. Molitor	1
Dr. Jay Hyman, MS RL 57	1
Dr. J. R. Beattie, MS RL 57	1
Dr. J. N. Matossian, MS RL 57	1
Princeton University Princeton, NJ 08540 Attn:	
Dean R. G. Jahn	1
Dr. Arnold Kelly	1
Boeing Aerospace Co. P. O. Box 3999 Seattle, WA 98124 Attn:	
Mr. Donald Grim, MS 8K31	1
Lockheed Missiles and Space Co. Sunnyvale, CA 94088 Attn:	
Dr. William L. Owens Dept. 57-24	1
Rocket Research Co. P.O. Box 97009 Redmond, WA 98073-9709 Attn:	
Mr. William W. Smith	1
Mr. Paul Lichon	1
Sandia Laboratories P. O. Box 5800 Albuquerque, NM 87185 Attn:	
Mr. Ralph R. Peters, Mail Code 4537	1
Mr. Dean Rovang, Mail Code 1251	1
Ion Tech Inc. 2330 E. Prospect Road Fort Collins, CO 80525 Attn:	
Dr. Gerald C. Isaacson	1
Dr. Dan Siegfried	1
Mr. Larry Daniels	1
EG & G Idaho P. O. Box 1625 Idaho Falls, ID 83401 Attn:	
Dr. G. R. Longhurst, TSA-104	1

	Copies
Michigan State University East Lansing, MI 48824 Attn:	
Dr. J. Asmussen	1
Dr. M.C. Hawley	1
Tuskegee Institute School of Engineering Tuskegee Institute, AL 36088 Attn:	
Dr. Pradosh Ray	1
Mr. Lee Parker 252 Lexington Road Concord, MA 01741	1
Physics Department Naval Postgraduate School Monterey, CA 93943-5000 Attn:	
Dr. Chris Olson, Mail Code 61-OS	1
Dr. Kevin Rudolph MS M0482 Martin Marietta Aerospace P. O. Box 179 Denver, CO 80201	1
Dr. Ira Katz Systems, Science and Software P. O. Box 1620 LaJolla, CA 92038	1
Dr. David Finkelstein Physics Department Georgia Institute of Technology Atlanta, GA 30332	1
Dr. Rod Burton G-T Devices, Inc. 5705 A General Washington Dr. Alexandria, VA 22312	1
Mr. Curtis Haynes Teletronix Inc. MS 50-431 P. O. Box 500 Beaverton, OR 97077	1
Electric Propulsion Laboratory, Inc. St. Rt. 2, Box 3406A Tehachapi, CA 93561 Attn:	
Dr. Graeme Aston	1
Dr. John R. Brophy	1